Computation of Periodic Solutions of Conservative Systems with Application to the 3-Body Problem

E. J. DOEDEL,* R. C. PAFFENROTH, H. B. KELLER,
ACM 217-50, California Institute of Technology,
Pasadena CA 91125, USA

D. J. DICHMANN,
Consultant, Torrance, CA, USA,

J. GALÁN-VIOQUE,
Matemática Aplicada II, Escuela Superior de Ingenieros,
Universidad de Sevilla, Camino de los Descubrimientos s/n,
Sevilla 41092, ESPAÑA

A. VANDERBAUWHEDE
Vakgroep Zuivere Wiskunde en Computeralgebra,
Universiteit Gent, Krijgslaan 281, B-9000 Gent, BELGIË

July 30, 2002

Abstract

We show how to compute families of periodic solutions of conservative systems with two-point boundary value problem continuation software. The computations include detection of bifurcations and corresponding branch switching. A simple example is used to illustrate the main idea. Thereafter we compute families of periodic solutions of the circular restricted 3-body problem. We also continue the figure-8 orbit recently discovered by Chenciner and Montgomery, and numerically computed by Simó, as the mass of one of the bodies is allowed to vary. In particular, we show how the invariances (phase-shift, scaling law, and x, y, z translations and rotations) can be dealt with. Our numerical results show, among other things, that there exists a continuous path of periodic solutions from the figure-8 orbit to a periodic solution of the restricted 3-body problem.

*Corresponding author. (On leave from Concordia University, Montreal). doedel@cs.concordia.ca

1 Introduction

There is much recent interest in new periodic solutions of the classical n-body problem of celestial mechanics. A particularly surprising solution is the one where 3 bodies follow each other along a single planar figure-8 orbit (see Fig. 15). The existence of this solution was proved by Chenciner & Montgomery [2000], and it was computed numerically by Simó. Simó has also discovered many other planar single-curve periodic solutions for $n \geq 3$ [Simó, 2000; Simó, 2002].

In this paper we show how two-point boundary value problem continuation software like AUTO [Doedel, 1981; Doedel *et al.*, 1997; Doedel *et al.*, 2000] can be used to compute families of periodic solutions of conservative systems, *i.e.*, systems having a first integral. The method is applicable to the computation of periodic solutions of the n-body problem and, in particular, to the numerical continuation of the figure-8 orbit, as the mass of one of the bodies is allowed to vary. The basic idea of the method is very simple, and for the case of one conserved quantity it was already used, without specific mention, in [Doedel, 1981], and subsequently in many other applications, for example, [Zufiría, 1987] and [Doedel *et al.*, 1991a].

First, in Sec. 2.1 and Sec. 2.2, we recall some basic notions of numerical continuation. In Sec. 2.3, we give a simple example to illustrate the principal idea used in the computation of families of periodic solutions of conservative systems. In Sec. 2.4 we state a mathematical result that illustrates justification of the general computational procedure under appropriate assumptions. A much more detailed theoretical treatment is given in [Muñoz-Almaraz *et al.*, 2002].

In Sec. 3 we apply the continuation method to the circular restricted 3-body problem (CR3BP). The mass-ratio parameter used in our calculations is approximately that of the Earth-Moon system. First we compute a family of planar periodic solutions of the CR3BP, namely, the Lyapunov orbits that originate from the libration point L1. Our calculation illustrates how easily these can be computed by numerical continuation until very close to a collision orbit. Then, in Sec. 3.2, we give graphical results that illustrate the rich solution structure of 3D periodic orbits in the CR3BP. Bifurcations are easily detected in our boundary value continuation approach, and lead to previously known and possibly new periodic orbits. The known orbits include the Halo orbits, whose behavior and stability properties have been computed before; see, for example [Howell, 1984] for a detailed numerical study. In Sec. 3.3 we discuss the use of libration point orbits in space mission design and we give some related references.

Our most elaborate application of the basic method for computing periodic orbits in conservative systems is presented in Sec. 4, where we continue the figure-8 orbit of Chenciner and Montgomery, as the mass of one of the bodies is allowed to vary. In Sec. 4.1 we show how the multiple invariances (phase-shift, scaling law, and x, y, z translations and rotations) can be dealt with. The local continuation of the figure-8 orbit, as the mass of one of the bodies is allowed to vary on a very small scale, is presented in Sec. 4.2. In Sec. 4.3 we discuss the global continuation of the figure-8 orbit, as the mass of one of the bodies varies between 1 and 0. Our numerical results show, among other things, that there exists a continuous path of periodic solutions from the figure-8 orbit to a periodic solution of the restricted 3-body problem.

2 Continuation of Solutions

Numerical continuation enables the computation of solution manifolds ("*solution families*"). Most existing algorithms are for the computation of one-dimensional solution manifolds ("*solution branches*"), see, e.g., [Rheinboldt, 1986; Doedel *et al.*, 1991b; Doedel *et al.*, 1991c; Seydel, 1995; Allgower & Georg, 1996; Beyn *et al.*, 2002], and [Kuznetsov, 1998] (Chapter 10), but continuation algorithms have also been developed for higher-dimensional manifolds; see, in particular, the recent paper by Henderson [2002], and references therein. In this paper we only consider the computation of solution branches.

2.1 Finite-dimensional systems

To recall the basic notions of continuation, first consider the finite-dimensional equation

$$F(X) = 0, \qquad F \ : \ \mathbb{R}^{n+1} \ \rightarrow \ \mathbb{R}^n, \tag{1}$$

where F is assumed to be sufficiently smooth. This equation has one more variable than it has equations. Given a solution X_0, one has, generically, a locally unique branch of solutions that passes through X_0. To compute a next point, say, X_1, on this branch, one can use Newton's method to solve the extended system

$$\begin{array}{ll} \text{a)} & F(X_1) = 0, \\ \text{b)} & (X_1 - X_0)^* \dot{X}_0 = \Delta s. \end{array} \tag{2}$$

Here $\dot{X}_0$ is the unit tangent to the path of solutions at X_0, the symbol * denotes transpose,

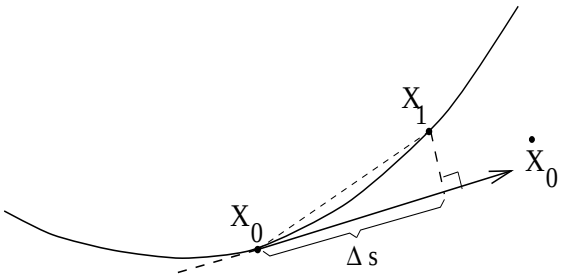

Figure 1: Pseudo-arclength continuation.

and Δs is a step size in the continuation procedure. The vector $\dot{X}_0$ is, of course, also a null vector of the Jacobian matrix $F_X(X_0)$, and can be computed at little cost [Doedel *et al.*, 1991b]. The geometrical interpretation of this well-known method, known as Keller's *pseudo-arclength method* [Keller, 1977], is shown in Fig. 1. The size of the pseudo-arclength step size Δs is normally adapted along the branch, depending, for example, on the convergence history of Newton's method.

It can be shown that the above continuation method works near a *regular solution* X_0, *i.e.*, if the null space of $F_X(X_0)$ is one-dimensional. In fact, in this case the Jacobian of (2) evaluated at X_0, *i.e.*, the $n+1$ by $n+1$ matrix

$$\begin{pmatrix} F_X(X_0) \\ \dot{X}_0^* \end{pmatrix}, \tag{3}$$

is easily seen to be nonsingular. By the Implicit Function Theorem, this guarantees the existence of a locally unique solution branch through X_0. This branch can be parametrized locally by Δs. Moreover, for Δs sufficiently small, and for sufficiently accurate initial approximation (e.g., $X_1^{(0)} = X_0 + \Delta s \dot{X}_0$), Newton's method for solving (2) can be shown to converge.

2.2 Periodic solutions

Here we recall how pseudo-arclength continuation can be used to compute a branch of periodic solutions of a dynamical system

$$x'(t) = f(x(t), \lambda), \qquad f \ : \ \mathbb{R}^n \times \mathbb{R} \ \rightarrow \ \mathbb{R}^n, \tag{4}$$

where $\lambda \in \mathbb{R}$ is a physical parameter. In this case the continuation step corresponding to Eq. (2) takes the form of the following constrained periodic boundary value problem:

$$\begin{array}{ll} \mathrm{a}_1) & \mathrm{x}_1'(\mathrm{t}) = \mathrm{T}_1 \mathrm{f}(\mathrm{x}_1(\mathrm{t}), \lambda_1), \\ \mathrm{a}_2) & \mathrm{x}_1(0) = \mathrm{x}_1(1), \\ \mathrm{a}_3) & \int_0^1 \mathrm{x}_1(\tau)^* \ \mathrm{x}_0'(\tau) \ \mathrm{d}\tau = 0, \end{array} \tag{5}$$

$$\mathrm{b}) \quad \int_0^1 (x_1(\tau) - x_0(\tau))^* \dot{x}_0(\tau) \ d\tau + (T_1 - T_0)\dot{T}_0 + (\lambda_1 - \lambda_0)\dot{\lambda}_0 = \Delta s.$$

This equation must be solved for $X_1 = (x_1(\cdot), T_1, \lambda_1)$, given a solution $X_0 = (x_0(\cdot), T_0, \lambda_0)$ and the path tangent $\dot{X}_0 = (\dot{x}_0(\cdot), \dot{T}_0, \dot{\lambda}_0)$. Here $T_1 \in \mathbb{R}$ is the unknown period. Equation ($5\mathrm{a}_2$) imposes unit periodicity, after rescaling of the independent variable t. Equation ($5\mathrm{a}_3$) is a phase condition, which fixes the phase of the new orbit $x_1(\cdot)$ relative to the given orbit $x_0(\cdot)$. It may be replaced by the classical Poincaré phase condition

$$\mathrm{a}_3') \quad (\mathrm{x}_1(0) - \mathrm{x}_0(0))^* \ \mathrm{x}_0'(0) = 0.$$

However, the integral phase condition ($5\mathrm{a}_3$) has the desirable property of minimizing phase drift relative to $x_0(\cdot)$, which often allows bigger continuation steps to be taken. Equation (5b) is the functional form of the pseudo-arclength constraint (2b). More details on this boundary value approach for computing periodic solutions can be found in [Doedel *et al.*, 1991c]; further references include [Doedel, 1981; Jepson, 1981; Doedel *et al.*, 1984].

In each continuation step Eq. (5) is solved by numerical boundary value algorithms. In particular, AUTO uses piecewise polynomial collocation with Gauss-Legendre collocation points ("*orthogonal collocation*") [de Boor & Swartz, 1973; Ascher *et al.*, 1995; Ascher & Petzold, 1998], similar to COLSYS [Ascher *et al.*, 1981], and COLDAE [Ascher & Spiteri, 1995], with adaptive mesh selection [Russell & Christiansen, 1978]. Combined with continuation, this allows the numerical solution of "difficult" problems, as illustrated by the near-homoclinic and near-collision orbits in this paper. (For other challenging applications see, for example, [Doedel, 1997].) Orthogonal collocation also has the desirable property of preserving the symplectic structure of Hamiltonian systems. AUTO determines the characteristic multipliers (or Floquet multipliers), that reflect asymptotic stability and bifurcation properties, as a by-product of the decomposition of the Jacobian of the boundary value collocation system [Doedel *et al.*, 1991c; Fairgrieve & Jepson, 1991]; see also [Lust, 2001].

2.3 A model conservative system

As a simple introductory example, consider the system

$$\begin{aligned} x_1' &= x_2, \\ x_2' &= -x_1(1-x_1), \end{aligned} \tag{6}$$

which has one first integral, namely the Hamiltonian $H(x_1, x_2) = \frac{1}{2}x_1^2 + \frac{1}{2}x_2^2 - \frac{1}{3}x_1^3$. This equation has a family of periodic solutions, of which representative orbits can be seen in Fig. 2_{center}. The family originates at $(x_1, x_2) = (0, 0)$, and terminates in a homoclinic orbit containing the saddle point equilibrium $(x_1, x_2) = (1, 0)$.

Note that Eq. (6) does not contain any parameters; yet it allows an entire family of periodic solutions. This non-generic behavior is typical for conservative systems. However, in Eq. (5) it is assumed that there is an explicitly available problem parameter, namely λ, which is part of the set of unknowns in each continuation step.

A straightforward approach to deal with this discrepancy is to use the conserved quantity (the Hamiltonian, in the example above), to eliminate one of the variables; then choose a suitable Poincaré section for the flow, and look for periodic orbits in the reduced problem. This scheme can be extended to the case of several constants of motion and has been extensively used in the literature, see, for example, [Simó, 1996]. It requires numerical integration of the differential equations, which can lead to instability in case of very stiff equations. Numerical integration is also difficult to apply to very unstable orbits. It also makes it difficult to use integral constraints, such as the integral phase condition ($5a_3$) and the continuation equation (5b), which have often significant computational advantages over pointwise constraints.

Another approach, adopted in this paper, is to reformulate the problem so that boundary value continuation methods can be applied. In our model problem this can be done by simply introducing an "unfolding" term, with unfolding parameter λ, for example,

$$\begin{aligned} x_1' &= x_2, \\ x_2' &= -x_1(1-x_1) + \lambda x_2. \end{aligned} \tag{7}$$

The unfolding term chosen here, corresponds to damping. When the damping parameter λ is zero then Eqs. (6) and (7) are identical. When λ is non-zero then all non-trivial periodic solutions disappear. Starting the computation from, for example, $\lambda = -1$, with $(x_1, x_2) = (0, 0)$, AUTO locates $(x_1, x_2, \lambda) = (0, 0, 0)$ as a Hopf bifurcation from the trivial solution, and then computes the emanating branch of periodic solutions at $\lambda = 0$ using the system (5). Along the periodic solution branch the value of λ, computed as part of the solution in each continuation step, will be zero (up to numerical precision). Figure 2_{top} shows the computed bifurcation diagram, in which the vertical axis is chosen to be the L_2-norm of the solution. Each point on the "vertical branch" in the bifurcation diagram represents a periodic solution. Note that there is no "distinguished" parameter in pseudo-arclength continuation; λ is just one of the quantities solved for in each continuation step. This allows the computation past folds and, as the current example illustrates, continuation of vertical solution branches.

As mentioned in Sec. 2.2, orthogonal collocation with adaptive mesh selection is used to solve the boundary value problem (5) at each continuation step. This allows the solution to be computed up to large periods; *i.e.*, until very close to the homoclinic orbit that terminates the branch. Periods as large as $T = 10^9$ are easily attained with a relatively small number of mesh intervals.

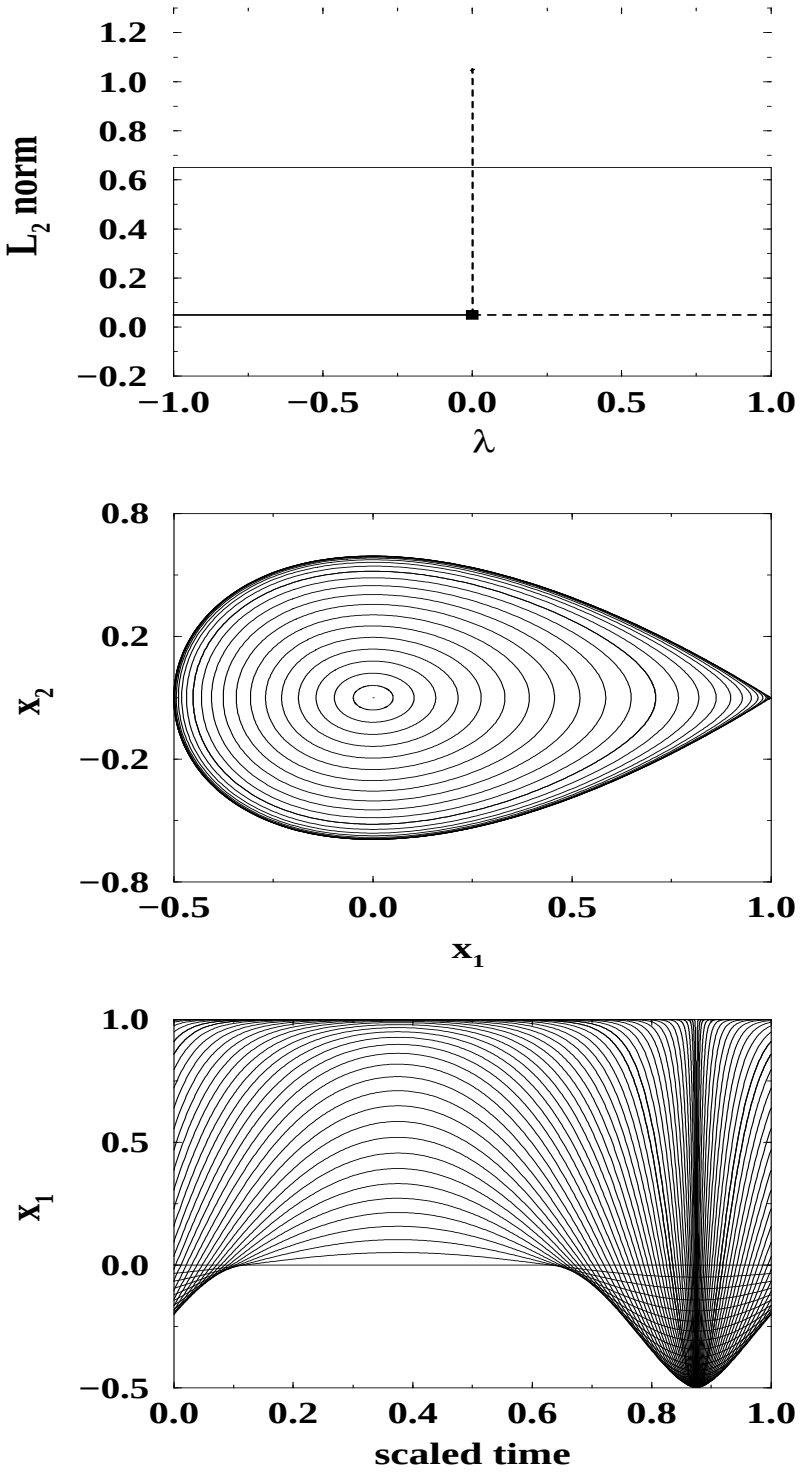

Figure 2: *Top:* Bifurcation diagram for Eq. (7), computed with AUTO. The vertical axis is the L_2 norm. For $\lambda \neq 0$ there are no non-trivial periodic solutions, while for $\lambda = 0$ there is a vertical branch of periodic orbits. The computed branch terminates near a homoclinic orbit where $||x|| = 1$. *Center:* Phase plane representation of some representative periodic orbits. *Bottom:* As a function of scaled time t, the solution component x_1 tends to a "downward delta function", which stays at practically the same location as the period T tends to infinity, due to the phase condition ($5a_3$).

Note that the integral phase condition ($5a_3$) has the property of keeping the "dip" in solution component x_1 at practically the same location when the period becomes large, as can be seen in Fig. 2_{bottom}. This allows much bigger continuation steps to be taken compared to phase conditions that allow this sharp dip to move.

The unfolding term in Eq. (7) was chosen on the basis of a physical argument, namely the effect of positive and negative damping. It is more satisfactory, however, to have a precise procedure for regularizing periodic orbit continuation in conservative systems. The general results in [Muñoz-Almaraz *et al.*, 2002]; (see Sec. 2.4 below) imply that the unfolding parameter times the gradient of the conserved quantity is an appropriate choice for the unfolding term. In the case of our test problem, Eq. (6), this gives the following alternate formulation that can be used to continue the periodic orbits:

$$\begin{aligned} x_1' &= x_2 + \lambda x_1(1 - x_1), \\ x_2' &= -x_1(1 - x_1) + \lambda x_2. \end{aligned} \tag{8}$$

2.4 A model result for conservative systems

Here we state a simple continuation result for the case of a conservative system with one conserved quantity. More general results are given in [Muñoz-Almaraz *et al.*, 2002]. Consider the dynamical system

$$x'(t) = f(x(t)), \qquad f \ : \ \mathbb{R}^n \ \rightarrow \ \mathbb{R}^n, \tag{9}$$

which has $C : \mathbb{R}^n \rightarrow \mathbb{R}$ as a conserved quantity, *i.e.*, $C(x(t))$ is constant along any orbit $x(t)$. Let $x_0(t)$ be a nontrivial periodic solution of Eq. (9) with period T_0. Finding a periodic solution with period T of Eq. (9) is equivalent to solving the boundary value problem

$$\begin{aligned} x'(t) &= T f(x(t)) + \lambda \nabla C(x(t)), \\ x(1) &= x(0), \end{aligned} \tag{10}$$

provided λ vanishes. For theoretical purposes, the continuation problem can be formulated as

$$p = x(1; p, T, \lambda), \tag{11}$$

where $x(t; p, T, \lambda)$ is the solution of Eq. (10) with $x(0) = p$ as initial condition. By hypothesis, $x_0(t)$ is a solution of Eq. (10) such that $x_0(1) = x_0(0)$, $T = T_0$ and $\lambda = 0$. Let $V(t)$ be the fundamental solution matrix of the variational equation, *i.e.*, $V(\cdot)$ satisfies

$$V'(t) = T_0 \ Df(x_0(t)) \ V(t), \qquad V(0) = I. \tag{12}$$

Using, for simplicity of presentation, the classical Poincaré phase condition ($5a_3'$), rather than the integral phase condition ($5a_3$), we can formulate the continuation problem as finding the zeros of

$$F(p, T, \lambda) = \begin{bmatrix} x(1; p, T, \lambda) - p \\ (p - x_0(0))^* x_0'(0) \end{bmatrix} . \tag{13}$$

The Implicit Function Theorem can now be used to prove the following:

Theorem 2.1 *Let x_0 be a solution of Eq. (10) whose monodromy matrix $V(1)$ has 1 as eigenvalue with geometric multiplicity 1. Then there exists a unique branch of solutions of $F(p, T, \lambda) = 0$ passing through $(x_0(0), T_0, 0)$. Moreover the parameter λ vanishes along this branch.*

The eigenvalues of $V(1)$ are the *Floquet multipliers* (or "characteristic multipliers") of the periodic orbit x_0 [Meyer & Hall, 1999]. We note that the algebraic multiplicity of the multiplier 1 is necessarily greater than one, for if it were equal to one then x_0 would be a locally unique periodic solution at $\lambda = 0$. The above theorem is essentially a computationally appropriate restatement of the cylinder theorem in conservative systems [Meyer, 1999]. It forms the basis for the justification of the simplest cases presented in this paper, namely, our model problem, and the continuation of periodic orbits in the restricted 3-body problem. Our computational results for the general three body problem, starting from the figure-8 orbit of Chenciner and Montgomery, requires an extension of the theorem to the case of a Hamiltonian system with several independent conserved quantities. General results of this nature are given in [Muñoz-Almaraz *et al.*, 2002].

3 The Restricted 3-Body Problem

The circular restricted 3-body problem (CR3BP) describes the dynamics of a body with negligible mass under the gravitational influence of two massive bodies, called the primaries, where the primaries move in circular orbits about their barycenter [Danby, 1992]. Let (x, y, z) denote the position of the negligible-mass body in a rotating barycentric coordinate system, where the x-axis points from the larger to the smaller primary; the z-axis is orthogonal to the orbital plane, and the y-axis completes the orthogonal coordinate system. The parameter μ represents the ratio of the mass of the smaller primary to the total mass. In this section we consider the Earth-Moon system, for which $\mu = 0.01215$. The units are chosen so that the distance between the primaries, the sum of the masses of the primaries, and the angular velocity of the primaries are all equal to one. The larger and smaller primaries are then located at $(-\mu, 0, 0)$ and $(1-\mu, 0, 0)$, respectively, and the equations of motion are given by

$$\begin{aligned} x'' &= 2y' + x - (1-\mu)(x+\mu)r_1^{-3} - \mu(x-1+\mu)r_2^{-3}, \\ y'' &= -2x' + y - (1-\mu)yr_1^{-3} - \mu y r_2^{-3}, \\ z'' &= -(1-\mu)zr_1^{-3} - \mu z r_2^{-3}, \end{aligned} \tag{14}$$

where

$$r_1 = \sqrt{(x+\mu)^2 + y^2 + z^2}, \qquad r_2 = \sqrt{(x-1+\mu)^2 + y^2 + z^2}.$$

This dynamical system has one integral of motion, namely the energy (or *Jacobi constant*)

$$E = (v_x^2 + v_y^2 + v_z^2)/2 - U(x, y, z) - \mu(1-\mu)/2 \ ,$$

where $v_x = x'$, $v_y = y'$, $v_z = z'$, and

$$U = \frac{1}{2}(x^2 + y^2) + \frac{1-\mu}{r_1} + \frac{\mu}{r_2} \ .$$

In accordance with Eq. (5) we rewrite Eq. (14) as a first order system, we scale time, so that the period T appears explicitly in the equations, and we add periodic boundary conditions and the integral phase constraint ($5a_3$). Following the discussion in the preceding section, we also introduce the unfolding term $\lambda \nabla E$. The resulting system of differential

equations is

$$\begin{aligned}
x' &= Tv_x + \lambda\ \partial E/\partial x,\\
y' &= Tv_y + \lambda\ \partial E/\partial y,\\
z' &= Tv_z + \lambda\ \partial E/\partial z,\\
v_x' &= T[2v_y + x - (1-\mu)(x+\mu)r_1^{-3} - \mu(x-1+\mu)r_2^{-3}] + \lambda\ \partial E/\partial v_x,\\
v_y' &= T[-2v_x + y - (1-\mu)yr_1^{-3} - \mu yr_2^{-3}] + \lambda\ \partial E/\partial v_y,\\
v_z' &= T[-(1-\mu)zr_1^{-3} - \mu zr_2^{-3}] + \lambda\ \partial E/\partial v_z.
\end{aligned} \tag{15}$$

3.1 Periodic orbits near the libration points

The phase space of Eq. (14) has an invariant subspace of planar orbits, for which $z = z' = 0$. The corresponding reduced system is given by

$$\begin{aligned}
x'' &= 2y' + x - (1-\mu)(x+\mu)r_1^{-3} - \mu(x-1+\mu)r_2^{-3},\\
y'' &= -2x' + y - (1-\mu)yr_1^{-3} - \mu yr_2^{-3},
\end{aligned} \tag{16}$$

where

$$r_1 = \sqrt{(x+\mu)^2 + y^2}, \qquad r_2 = \sqrt{(x-1+\mu)^2 + y^2}.$$

It is well known that for each value of μ Eq. (16) (and Eq. (14)) has five equilibria in the orbit plane of the primaries, called *Lagrange points* or *libration points* [Szebehely, 1967; Gómez *et al.*, 2001b; Gómez *et al.*, 2001c]. Three of the libration points, denoted L1, L2 and L3, are collinear with the primary bodies; one of them, L1, lies between the primaries. In the case of the Earth-Moon system, for which $\mu = 0.01215$, L2 is the libration point beyond the moon, while L3 is the libration point beyond the earth. Each of the other two points, L4 and L5, forms an equilateral triangle with the primaries. All five libration points can be seen in the schematic bifurcation diagram in Fig. 4, which will be discussed in detail in Sec. 3.2 below.

The libration points L1, L2, L3, each give rise to a family of planar periodic orbits, the Lyapunov orbits. Computational results for the Lyapunov orbits that emanate from L1 are shown in Fig. 3. As solutions to (Eq. (16)), *i.e.*, as orbits in 4-dimensional phase space, these orbits are unstable, with two Floquet multipliers equal to 1, one real multiplier greater than one, and one real multiplier less than one.

However, as orbits in 6-dimensional phase space, *i.e.*, as solutions of Eq. (14), there are various bifurcations from the Lyapunov orbits. On portions of the solution branch the orbits have complex multipliers that move around the unit circle in the complex plane, as can be determined numerically using AUTO, giving rise to invariant tori, sub-harmonic bifurcations and period-doubling bifurcations. There are also *bifurcation points*[1], where distinct solution branches intersect, with identical orbit and period at the point of intersection. (Recall that, in our continuation setting, a periodic solution X has components $(x(\cdot), T, \lambda)$, where x denotes the orbit, T is the period, and where the unfolding parameter λ is zero along the solution branch.)

Moreover, in the full 6-dimensional model, the Jacobian at the libration points L1, L2, and L3 has two pairs of purely imaginary eigenvalues, giving rise to a second branch of well-known periodic solutions, namely the so-called Vertical orbits [Howell, 2001]. Furthermore, for μ less than a critical value, $\mu_1 \equiv 1/2 - \sqrt{23/108} \approx 0.0385$, each of the libration points L4 and L5 gives rise to three families of periodic solutions. In the numerical results below

[1]In this paper we reserve the term *bifurcation point* (or *bifurcation orbit*), when not further qualified, for transcritical and pitch-fork bifurcations, excluding period-doubling, torus, and subharmonic bifurcations.

we restrict our presentation to the Lyapunov and Vertical families from L1, and some of the branches that bifurcate from them. We do not present results here on branches of periodic solutions that bifurcate from subharmonic- and period-doubling bifurcations. The solution structure that we present can be viewed as a "skeleton" [Deprit & Henrard, 1969], from which many other solutions may be reached. Also, to keep the presentation relatively simple, we do not present results for the planar and Vertical families that originate from L2 and L3. Some of the branches that we present lead to L4 and L5; however, we also omit results for the remaining two families that emanate from each of L4 and L5.

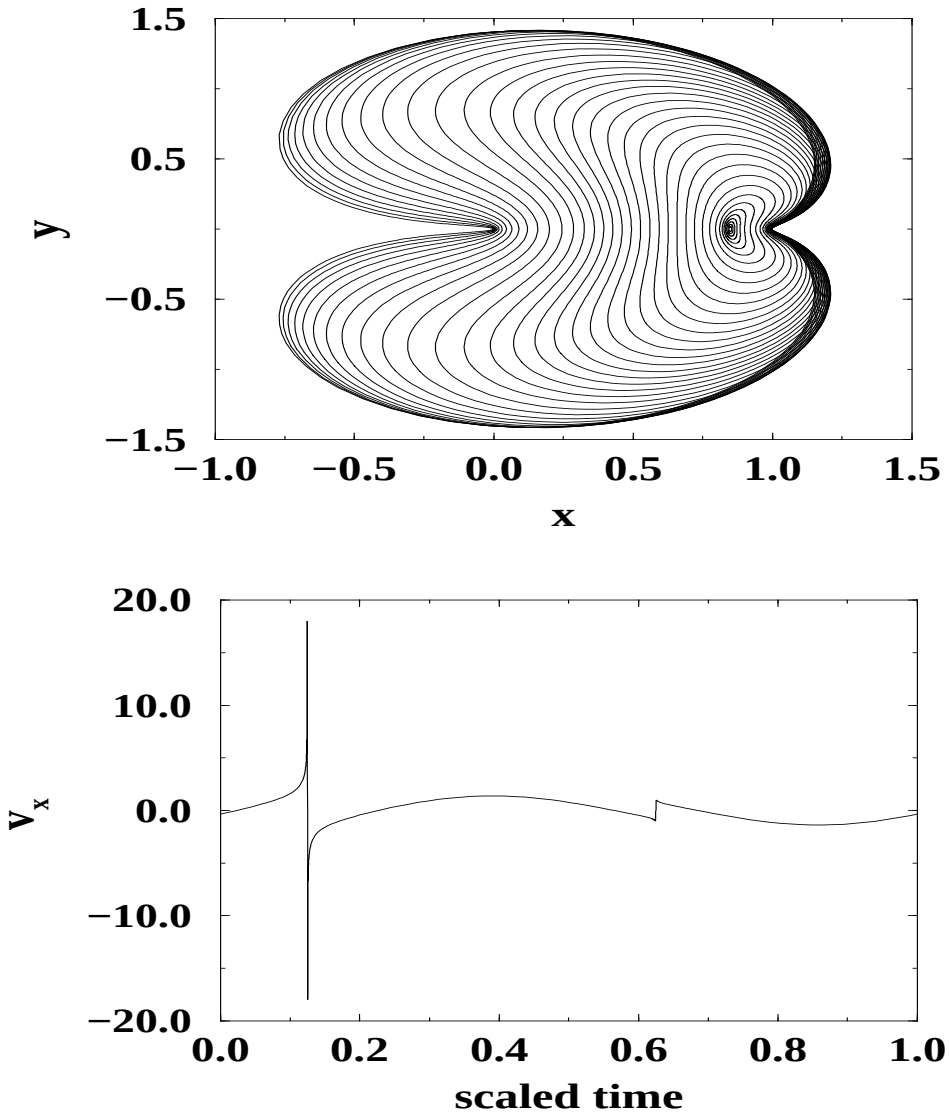

Figure 3: *Top:* $x - y$ representation of a selection of Lyapunov orbits. The smallest orbits are close to L1, while the largest orbits are near collision. The Earth and the Moon are located at $(-\mu, 0)$ and $(1 - \mu, 0)$, respectively, where $\mu = 0.01215$. *Bottom:* Velocity component $v_x(t)$ as a function of scaled time t for a near-collision orbit. Note the rapid changes of $v_x(t)$ near the Earth and near the Moon. (The highest velocity along the orbit occurs near the Earth.)

3.2 A tour of the bifurcation diagram

Here we explain the bifurcation diagram in Fig. 4. The solution branches shown are those obtained by following the two branches of periodic orbits that emanate from L1, and subsequent branches that originate at bifurcation points along computed branches.

In Fig. 4 we use colored curves to represent various families of periodic solutions. For reference, Fig. 4 and later figures in this section show the Earth and Moon as two textured spheres. The five libration points are shown as grey cubes, and families of periodic orbits are shown emanating from the appropriate cube. For example, the red line of Lyapunov orbits emanates from the cube representing L1. All bifurcation points are marked as small white spheres except for four brown colored bifurcation points at which we do not display the bifurcating branches. In addition, we include a grey rectangle in the $x-y$ plane. Any solution branch that touches this plane has a planar solution at that point. For example, since the entire branch of Lyapunov orbits is planar, the entire red line lies in the grey plane. We emphasize that even though the various visualization aids are in the proper physical position with respect to each other; the bifurcating branches themselves are only schematic. The relative positions of the various bifurcating branches should not be interpreted as signifying any physical property of the solutions, other than those discussed above.

As mentioned, the red line in Fig. 4 emanating from L1 represents the Lyapunov orbits. Two bifurcation points are shown along the path of Lyapunov orbits, the first giving rise to the blue family of Halo orbits (see Figs. 9 and 10). On the green curve of Vertical orbits (see Figs. 6 and 7) there is a bifurcation point which gives rise to a yellow family of orbits that connects to the second bifurcation point on the Lyapunov family (see Fig. 11). On the blue curve of Halo orbits there are two symmetry related bifurcation points giving rise to the cyan family of orbits (see Fig. 12). The cyan family of orbits has two symmetry related bifurcation points which give rise to the magenta family of orbits, which connects the "Vertical" orbits emanating from L4 and L5 (see Figs. 13 and 14). There is a brown colored bifurcation point on this branch through which one can reach L3 as well, although this connecting branch is not shown here.

We begin our tour of the periodic orbits by discussing several well-known families which emanate from L1, as shown in Fig. 5. Previous work has mapped portions of the families of periodic orbits for various values of μ; cf. [Howell, 2001] and references therein. Several authors have investigated bifurcations of these families, including [Hadjidemetriou, 1975; Ichtiaroglou & Michalodimitrakis, 1980; Markellos, 1981] and [Hénon, 1997; Hénon, 2001; Howell & Campbell, 1999]. The red plane in Fig. 5 contains a subset of small-amplitude Lyapunov orbits from Fig. 3 near L1, with selected individual orbits shown as curves. Similarly, the green surface contains Vertical orbits and the blue surface contains Halo orbits. The coloring scheme is the same as used in Fig. 4. As a visualization aid we show orbits from which other families of periodic orbits bifurcate as thickened tubes. Accordingly, the thick blue orbit which lies in the plane of the Lyapunov orbits is the orbit from which the Halos bifurcate. To reduce clutter in the diagram we have only plotted the "northern" Halo orbits and not the symmetry related "southern" Halo orbits which are a mirror image of the "northern" Halo orbits reflected across the $x-y$ plane.

We now turn our attention to the green Vertical orbits. In Fig. 6 we show the Vertical orbits from their origin at L1 up to their first bifurcation point. In this and all following figures in this section the bifurcation diagram from Fig. 4 is shown on the right, with the appropriate branch portion indicated by a white arrow. As before, the bifurcation orbit is shown as a

thickened tube. Similarly, Figs. 7 and 8 show the family of Vertical orbits starting at the first bifurcation point. As can be seen, these orbits grow to encompass the Earth-Moon system, and end in a period-doubling bifurcation from a family of planar solutions. Accordingly, the green curve in Fig. 4 touches the grey plane in two places; the first corresponding to the creation of the family at L1 and the second at the period-doubling bifurcation from a planar solution (B2 in Fig. 7).

There are two bifurcation points on the green branch of Vertical solutions away from planar solutions. As can be seen in Fig. 4, the first bifurcating branch connects the red Lyapunov and green Vertical families, and the orbits themselves are shown in yellow in Fig. 11. The red plane is a collection of Lyapunov orbits and the thick planar orbit is the second bifurcation orbit on the Lyapunov family. The thick green orbit is the first bifurcation orbit on the Vertical branch, as shown in Fig. 6. The yellow orbits are a representative collection of orbits which connect these two bifurcation orbits. Some of the orbits on the "Y" branch were plotted in Zagouras and Kazantzis for the Sun-Jupiter case [Zagouras & Kazantzis, 1979]. There is a second symmetry related branch not shown here, and the whole family of orbits forms a loop as shown in Fig. 4.

The first bifurcation point on the red Lyapunov branch gives rise to the well-known Halo orbits; see [Farquhar & Kamel, 1973; Breakwell & Brown, 1979], and [Howell, 1984; Howell & Farquhar, 1993; Howell, 2001]. Figure 9 shows a selection of "northern" Halo orbits between the bifurcation point on the Lyapunov branch from which they arise up to the first bifurcation point on the Halo family itself. We have removed the surface of orbits from this figure in order to make the two bifurcation orbits easier to distinguish. Figure 10 begins where Fig. 9 ends and shows the "northern" Halo orbits from the first bifurcation point on the Halo branch up to the second bifurcation point which gives rise to a planar family of solutions, not shown here. As can be seen in Fig. 4, the Halo branch can be continued past the planar bifurcation point to obtain the symmetry related branch of "southern" Halos. Accordingly, the blue family of Halo orbits in Fig. 4 is a loop.

As is evident, the connectivity of the bifurcation diagram is quite complex. On the branch of Halo orbits there are two symmetry related bifurcation points. They are connected by the cyan loop of orbits shown in Fig. 4. Two additional symmetry related bifurcation points occur on the cyan loop, and they give rise to the magenta branch which twice intersects the cyan loop transcritically.

On the cyan loop there are four symmetric segments separated by the four bifurcation points. Figure 12 shows a representative collection of orbits on the cyan loop from one of these segments. The other segments have the same structure as Fig. 12 except that they are reflected across the $x-y$ plane and/or the $x-z$ plane. The small thick cyan orbit corresponds to the larger bifurcation orbit in Fig. 9. The thick cyan figure eight orbit in the middle of Fig. 12 is a bifurcation orbit and connects with the magenta family.

The magenta family of orbits is of particular interest in that it connects the "Vertical"-like orbits from L4 with the "Vertical"-like orbits from L5. In fact, the "Vertical" orbits of L4 and L5 are the same family of orbits. The magenta family of orbits transcritically intersects the cyan family of orbits in two places, and there is a third bifurcation point in between these two (shown as the brown bifurcation point in Fig. 4).

Figure 13 shows a representative collection of orbits emanating from L4 which are very similar to the Vertical orbits which emanate from L1. The thick magenta orbit is the same bifurcation orbit as shown in Fig. 12, and is the first bifurcation point one encounters on the magenta branch as one moves away from L4.

Figure 14 shows a representative collection of orbits between the figure eight bifurcation orbit shown in Figs. 12 and 13 and the brown bifurcation point on the magenta family. The thick magenta orbit, which encompasses the Earth, is a bifurcation orbit which connects to the "Vertical" orbits of L3, though this branch of orbits is not shown here. This bifurcation point is shown in brown in Fig. 4. Continuation of the branch past the brown bifurcation point gives a symmetry related family of "Vertical" orbits for L5. This family consists of the symmetric version of Figs. 13 and 14 reflected through the $x - z$ plane.

The family of magenta orbits shown in Fig. 13 is the Vertical family emanating from L4; an analogous Vertical family emanates from L5. Zagouras [1985] used Poincaré-Lindstedt series to study the continuation and bifurcation of the Vertical families emanating from the equilateral libration points for the Sun-Jupiter case. Zagouras traced the Magenta family of orbits from L4 to the Vertical family emanating from L5, and identified the bifurcation points that we call L4V and L45 shown in Fig. 14. Zagouras identified L45 as a branch point to the Vertical family emanating from L3, and numerically continued the family branching from L4V which we call the Cyan family. The work in [Zagouras, 1985] was extended in [Papadakis & Zagouras, 1992] to consider the families of three-dimensional periodic orbits for other values of μ.

For μ less than the critical value $\mu_1 \approx 0.0385$ there are planar periodic orbits emanating from L4 and L5 [Danby, 1992; Szebehely, 1967]. Also, L4 and L5 are linearly stable in the CR3BP for $\mu < \mu_1$. Astronomers have therefore looked to see whether natural satellites exist near the equilateral points in the solar system. The so-called Trojan asteroids have been observed near the equilateral points in the Sun-Jupiter and Sun-Mars systems. In addition, the equilateral points play a role in the intricate dynamics of Saturn's moon and ring system [Murray & Dermott, 1999]. The families of planar periodic orbits and their bifurcations emanating from L4 and L5 have been studied extensively for subcritical values of μ. See in particular [Deprit & Henrard, 1968; Deprit & Henrard, 1970; Gómez & Noguera, 1985; Gómez *et al.*, 2001b]. Ragos *et al.* [1997] examined the planar families around the equilateral libration points for values of μ both below and above the critical value μ_1.

Although our numerical results in this section are limited to the Earth-Moon system, we have also applied the techniques to other values of the mass-ratio parameter μ. In fact, these calculations can be automated by means of *scripts* [Doedel & Paffenroth, 2001] that generate bifurcation diagrams similar to that in Fig. 4 for any given value of μ. Moreover, these automated calculations can be made to follow all branches that emanate from each of the five libration points. Furthermore, one can use numerical continuation of singular points to follow the bifurcation points as μ is allowed to vary. We do not report these more extensive results in this paper; however, below we do include a discussion of the relevance of libration points and their associated periodic orbits in actual space mission design.

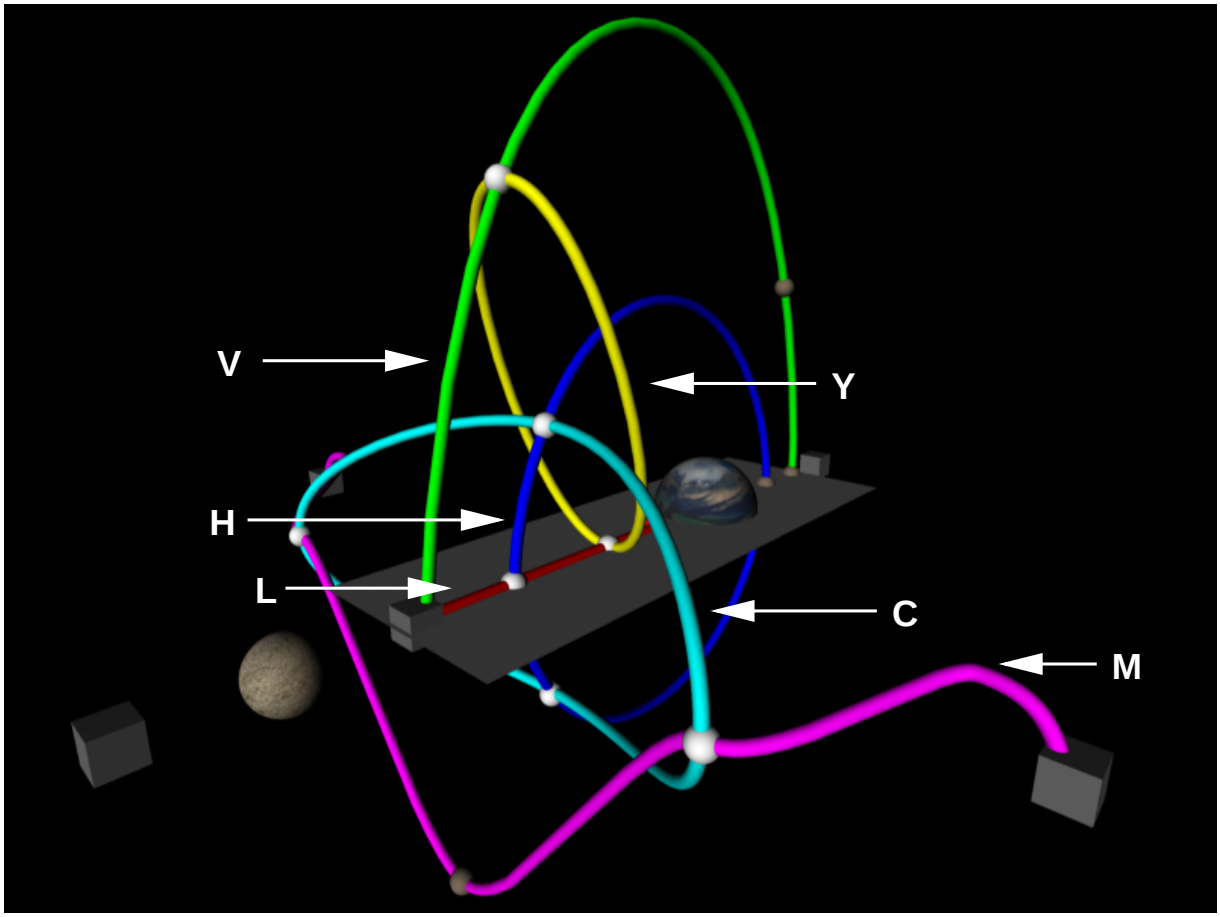

Figure 4: Schematic bifurcation diagram of periodic orbits emanating from L1 and from subsequent bifurcation points. The five libration points are shown as grey cubes. The red line (labeled L) represents the Lyapunov orbits and the green curve (V) represents the Vertical orbits (see Figs. 6, 7, and 8). Any solution branch that touches the grey plane has a planar periodic solution at that point. The red line of Lyapunov orbits shows two bifurcation points, the first gives the blue family (H) of Halo orbits (see Figs. 9 and 10) and the second gives the yellow (Y) family of orbits that connects the Lyapunov and Vertical families (see Fig. 11). The two symmetry related bifurcation points on the blue curve of Halo orbits give rise to the cyan (C) family of orbits (see Fig. 12). The cyan family of orbits has two symmetry related bifurcation points which give rise to the magenta (M) family of orbits, which connects the "Vertical" orbits emanating from L4 and L5 (see Figs. 13 and 14).

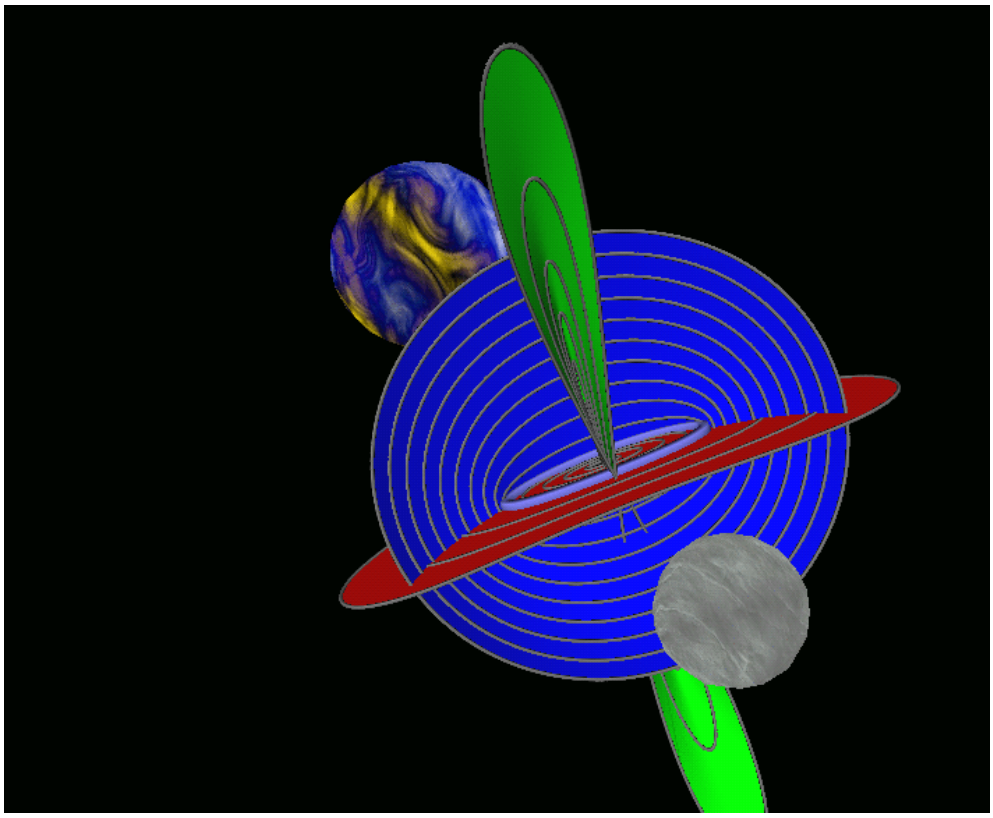

Figure 5: Some well-known periodic orbits: The red plane consists of Lyapunov orbits, with selected orbits shown as curves. Similarly, the green surface consists of Vertical orbits, and the blue surface of "northern" Halo orbits. The coloring scheme is the same as used in Fig. 4. The thick blue orbit is the Lyapunov orbit from which the Halos bifurcate. The symmetry related family of "southern" Halo orbits is not shown.

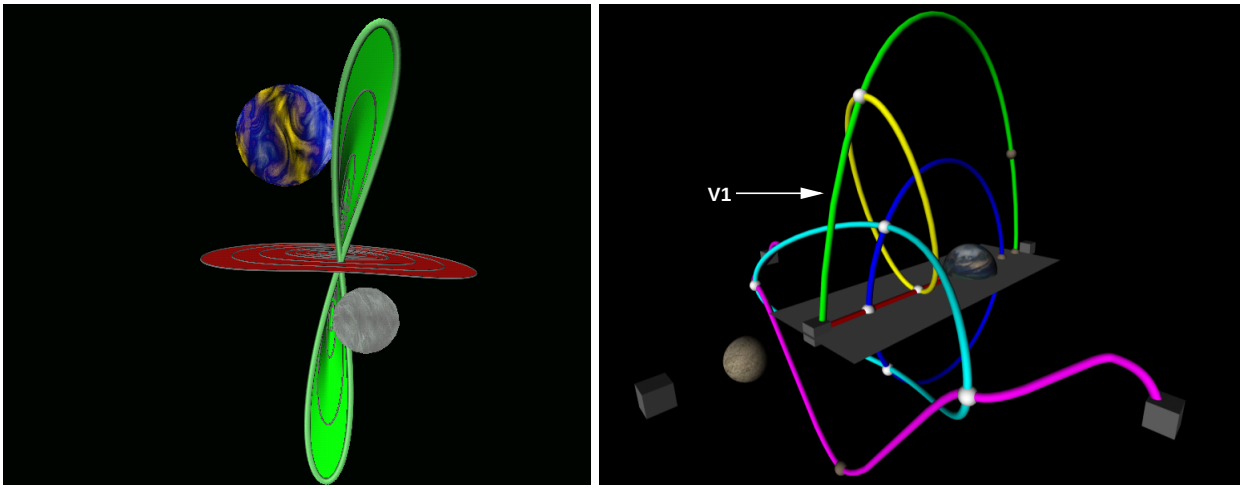

Figure 6: The Vertical orbits up to the first bifurcation point: The green surface contains all Vertical orbits up to the first bifurcation point, which is shown as a thick green orbit. The part of the bifurcation diagram where these orbits are found is indicated on the right by a white arrow.

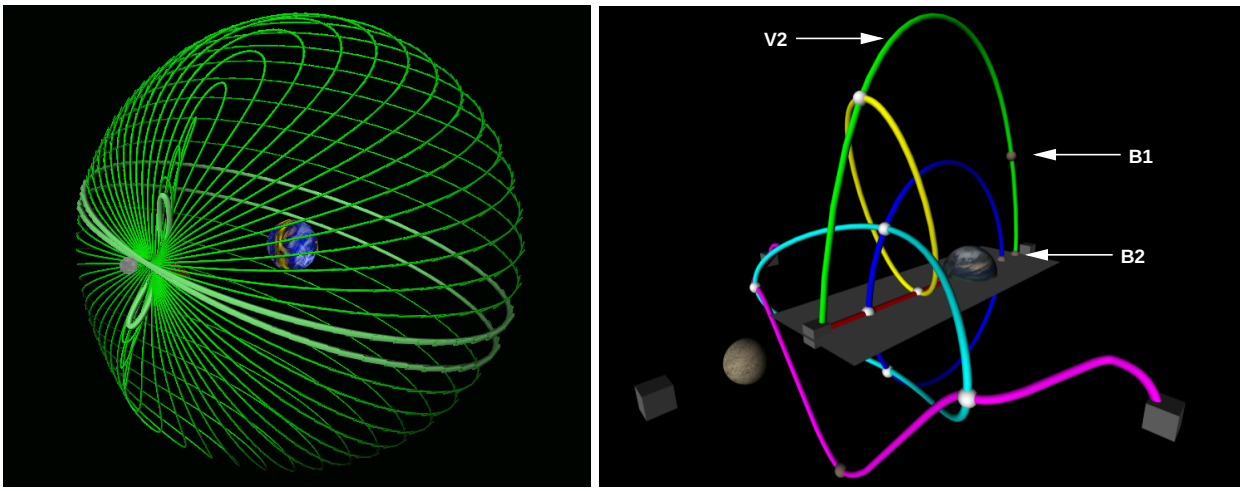

Figure 7: An overall view of the Vertical orbits on the indicated branch portion (V2), between the white and the brown (B1) bifurcation points. The orbits at the bifurcation points are shown as a thick green orbits. The branch of Vertical orbits connects via a "reverse period-doubling" (B2) to a family of circular planar orbits (not shown) just beyond the second bifurcation point (B1). The branch bifurcating from B1 is not shown.

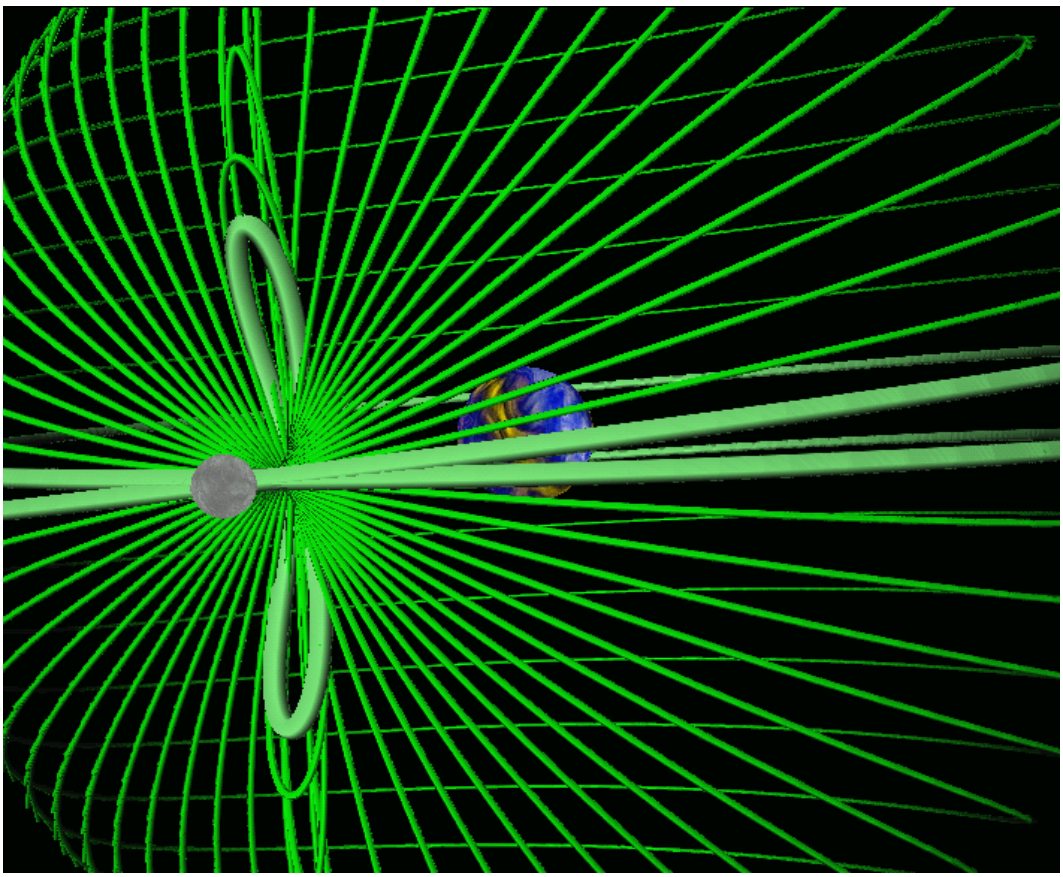

Figure 8: A closeup view of the Vertical orbits near the first (white) bifurcation point in Fig. 7.

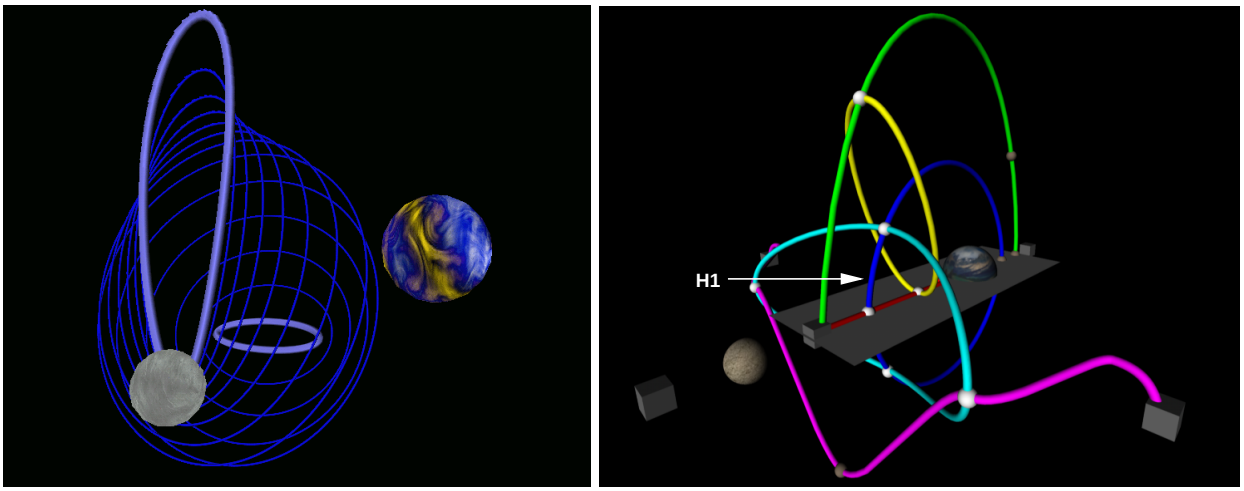

Figure 9: The Halo orbits (H1) up to the first bifurcation point: The blue curves are a representative collection of orbits from the "northern" families of Halo orbits. The thick blue orbit between the Earth and Moon is the Lyapunov orbit from which the Halo orbits bifurcate. The thick blue orbit near the Moon is the first bifurcation point on the branch of Halo orbits.

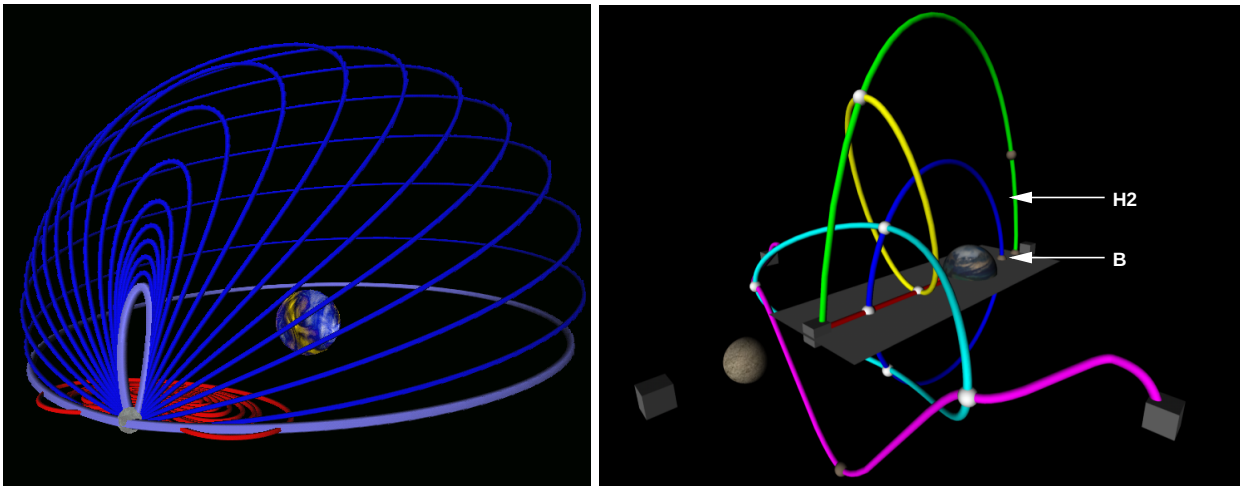

Figure 10: The "northern" Halo orbits (H2) after the first bifurcation point. For reference, a set of red Lyapunov orbits is also shown. The thick blue orbit near the Moon is the first bifurcation point on the branch of "northern" Halo orbits. The thick blue orbit which encompasses the Earth is a bifurcation point to a family of planar orbits which is not shown here. Also not shown are the symmetry related "southern" Halo orbits, although the corresponding branch does appear in the bifurcation diagram.

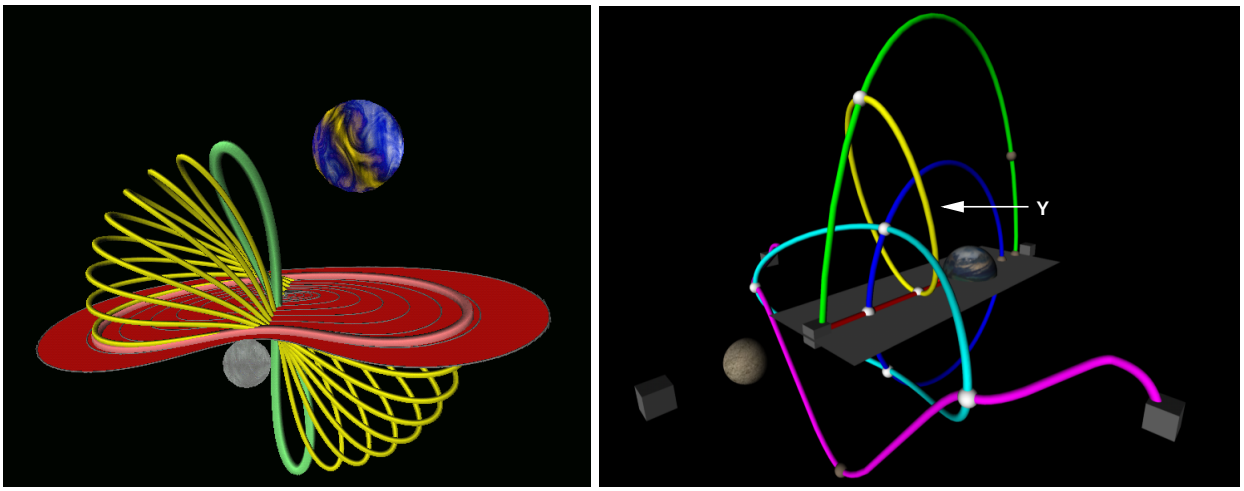

Figure 11: A family of orbits (Y) connecting the Lyapunov and Vertical orbits. The red plane is a collection of Lyapunov orbits and the thick red orbit is the second bifurcation point in the Lyapunov family. The thick green orbit is the first bifurcation point on the Vertical branch, as also shown in Fig. 6. The yellow orbits are a representative collection of orbits which connect these two bifurcation points. There is a second symmetry related branch not shown here which consists of the above orbits reflected across the $x - z$ plane. Accordingly, the whole family of orbits forms a loop as shown in Fig. 4.

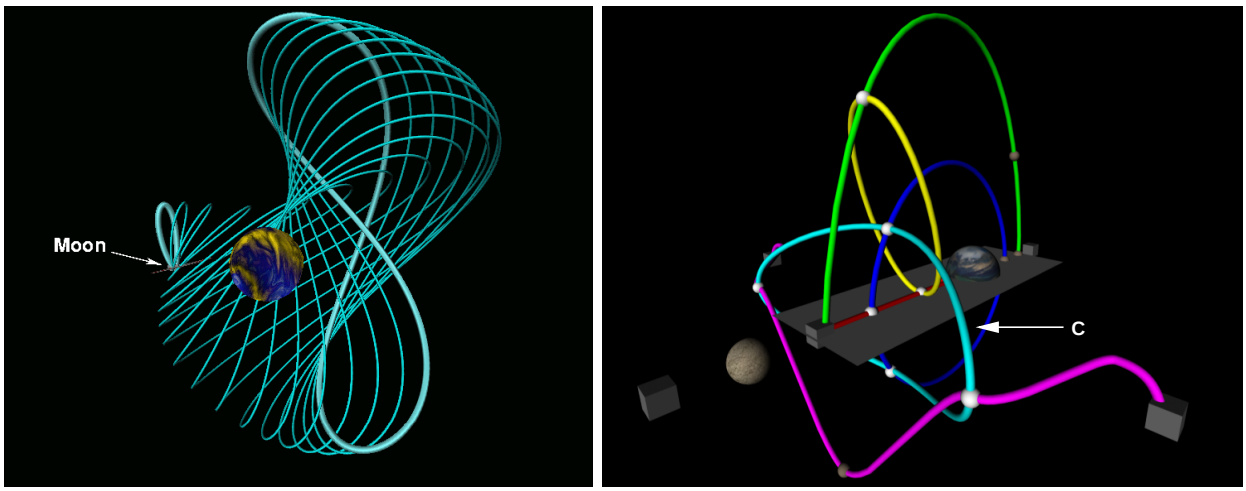

Figure 12: The cyan curves are a representative collection of orbits which emanate from the first bifurcation point on the Halo family. The elliptical bifurcation orbit close to the Moon from Fig. 9 corresponds to the small thick cyan orbit. The thick cyan figure eight orbit in the middle of the figure is a bifurcation orbit that connects with a family of "Vertical"-like orbits which emanates from L4.

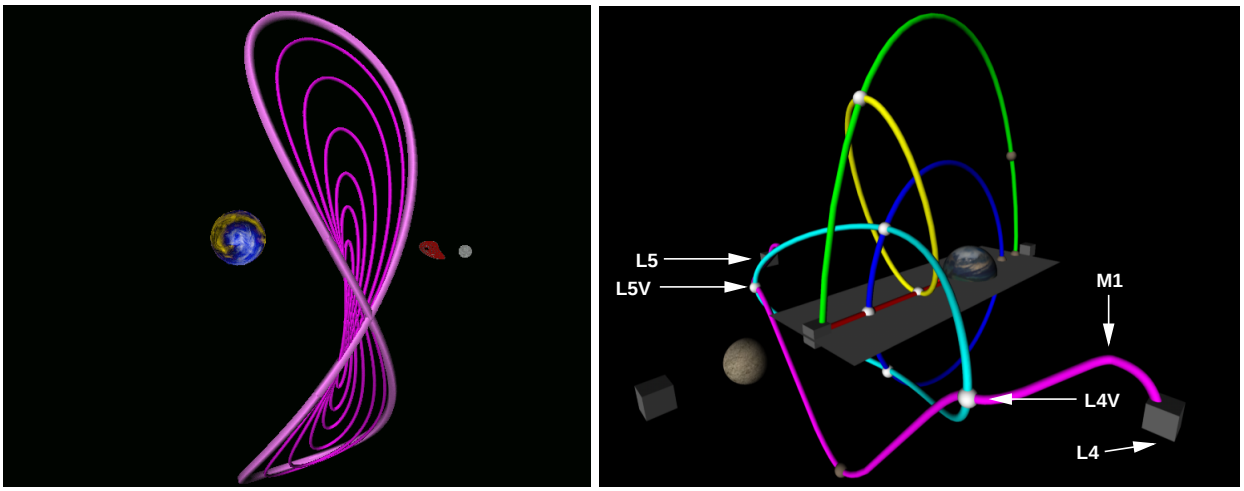

Figure 13: The L4 "Vertical" orbits: The magenta curves are a representative collection of orbits emanating from L4 which are very similar to the Vertical orbits that emanate from L1. There are two families of such orbits and the ones shown here (M1) can be found in the bifurcation diagram between the white arrows marked "L4" and "L4V". The other family is found in the bifurcation diagram between the white arrows marked "L5" and "L5V". The thick magenta orbit is the same bifurcation orbit shown in Fig. 12.

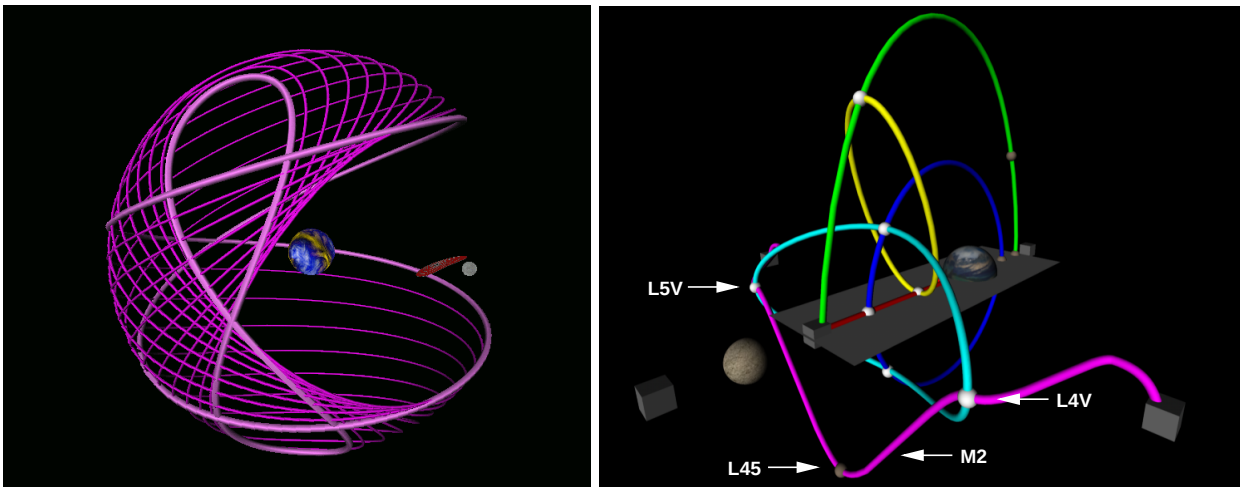

Figure 14: The magenta curves are a representative collection of orbits between the bifurcation points marked "L4V" and "L45". The thick magenta orbit, which encompasses the Earth, is the bifurcation point marked "L45". This orbit connects to the "Vertical" orbits of L3 which are not shown here. Continuing on the branch past "L45" one reaches the symmetric image of "L4V", namely "L5V", which connects to the "Vertical" orbits for L5.

3.3 Libration point orbits in the solar system

As noted above, the periodic orbits around the equilateral libration points are significant in the solar system dynamics. In addition, some of the libration point orbits discussed above have been or could be exploited in space mission design. Due to the fixed positions of L1 and L2 along the line between the primaries in the rotating frame, the regions around L1 and L2 provide excellent locations for scientific observation spacecraft and for communication relays [Farquhar, 1968; Farquhar & Dunham, 1990; Farquhar, 2001] analogous to the geostationary communications relays already proposed in [Clarke, 1945; Clarke, 1947].

In 1978, the NASA International Sun-Earth Explorer 3 (ISEE-3) became the first spacecraft to orbit the Sun-Earth L1 point, where it traced a Halo orbit [Farquhar, 2001]. The Halo orbits for the ISEE-3 mission were computed using the Lindstedt-Poincaré method, combined with Newton's method, to provide an accurate first approximation [Farquhar & Kamel, 1973; Breakwell & Brown, 1979; Richardson, 1980].

Since that time, the European Space Agency (ESA)/NASA SOHO mission and the NASA ACE mission have used Halo orbits about the Sun-Earth L1 point for solar observations [Rodriguez-Canabal & Hechler, 1989; Farquhar, 2001]. It is known that the libration points L1 and L2 are linearly unstable in the CR3BP for all values of μ [Danby, 1992], and the Halo orbits used for these missions are themselves unstable. Nevertheless, a spacecraft can remain in orbit around the Sun-Earth L1 or L2 point for years by performing small maneuvers every few months [Dunham & Roberts, 2001]. Recent libration point mission design has exploited dynamical systems theory to compute stable, unstable and center manifolds for libration point orbits [Howell *et al.*, 1997; Gómez *et al.*, 2001a]. In 2001 the MAP spacecraft was placed in orbit about the Sun-Earth L2 point [Folta & Richon, 1998]. Due to mission constraints the MAP mission does not use an orbit from the Halo family, because the minimum amplitude of the Halo family in the $x-y$ plane is too large. Instead MAP uses a smaller, quasiperiodic orbit. The Genesis mission, launched in 2001, calls for the spacecraft to first orbit the Sun-Earth L1 point, then follow a heteroclinic connection to an orbit around L2 before returning to Earth [Koon *et al.*, 1999; Koon *et al.*, 2000; Lo *et al.*, 2001]. Some other scientific missions that are planned to orbit the Sun-Earth L2 point are NASA's Next Generation Space Telescope (NGST) [Folta *et al.*, 2001a] and ESA's FIRST and Planck missions [Felici *et al.*, 2001]. In a more elaborate design, the Terrestrial Planet Finder (TPF) mission will exploit the center manifold of a Halo orbit to fly two spacecraft in formation along Lissajous orbits about the Sun-Earth L2 point [Gómez *et al.*, 1997; Barden & Howell, 1998; Gómez *et al.*, 2001d]. The large Vertical orbits shown in Fig. 7 may also be useful to observe the Earth's polar regions [Folta *et al.*, 2001b].

During NASA's Apollo program, it was proposed that an orbit about the Earth-Moon L2 point be used for a relay satellite that would allow a lander on the far side of the Moon to communicate with Earth [Farquhar, 1968; Farquhar, 2001]. This innovative concept was never implemented. Recently a related study has considered placing spacecraft in orbits about the Sun-Mars L1 and L2 points to support communications between Mars landers and Earth [Strizzi *et al.*, 2001].

4 The General 3-Body Problem

Since the formulation of the law of gravitation by Newton, the 3-body problem of celestial mechanics has been one of the most studied problems in physics and mathematics. It is easy enough to state; in fact, the equations are given by

$$\begin{aligned}
\mathbf{x}_1'' &= -m_2 \frac{\mathbf{x}_1 - \mathbf{x}_2}{|\mathbf{x}_1 - \mathbf{x}_2|^3} - m_3 \frac{\mathbf{x}_1 - \mathbf{x}_3}{|\mathbf{x}_1 - \mathbf{x}_3|^3} \ , \\
\mathbf{x}_2'' &= -m_1 \frac{\mathbf{x}_2 - \mathbf{x}_1}{|\mathbf{x}_1 - \mathbf{x}_2|^3} - m_3 \frac{\mathbf{x}_2 - \mathbf{x}_3}{|\mathbf{x}_2 - \mathbf{x}_3|^3} \ , \\
\mathbf{x}_3'' &= -m_2 \frac{\mathbf{x}_3 - \mathbf{x}_2}{|\mathbf{x}_3 - \mathbf{x}_2|^3} - m_1 \frac{\mathbf{x}_3 - \mathbf{x}_1}{|\mathbf{x}_1 - \mathbf{x}_3|^3} \ ,
\end{aligned} \tag{17}$$

where $\mathbf{x}_i \equiv (x_i, y_i, z_i)^*$, and where m_i denotes the mass of the ith body. This equation can be written as a system of eighteen first order differential equations. It has seven independent conserved quantitites, namely, the Hamiltonian, the three components of the linear momentum $\mathbf{P} = \sum_{i=1}^{3} m_i \mathbf{x}_i'$, and the three components of the angular momentum $\mathbf{L} = \sum_{i=1}^{3} m_i \mathbf{x}_i \wedge \mathbf{x}_i'$.

Despite its apparent simplicity, it has been notoriously difficult to obtain detailed information on the global solution structure of Eq. (17). In particular, much effort has been devoted to the study of periodic solutions; see, for example, [Hadjidemetriou, 1975; Arenstorf, 1976; Meyer, 1981a; Davoust & Broucke, 1982; Meyer, 1999; Bruno, 2001]. One well-known periodic solution is the Lagrange equilateral triangle solution, in which three equal-mass bodies are located at the vertices of an equilateral triangle that rotates with constant angular velocity; the three bodies thereby describing a circle. Another well-known periodic solution is Euler's collinear solution, where two bodies rotate at constant angular velocity around a circle, while the third body is at rest at the centre.

In a spectacular discovery, Chenciner & Montgomery [2000] recently proved the existence of the planar figure-8 periodic solution of the equal-mass 3-body problem shown in Fig. 15. Such a solution had earlier been predicted by Moore [1993]. The proof uses variational arguments; after certain reductions the action integral is minimized over a restricted set of symmetric arcs. The variational argument does not provide the stability properties of the figure-8 solution. However, Simó [2000] numerically computed this remarkable solution with great accuracy, and determined *elliptic stability*; *i.e.*, the Floquet multipliers of the periodic orbit are on the unit circle in the complex plane. As will be seen in Sec. 4.2, elliptic stability is preserved for very small changes (of the order 10^{-5}) in one of the masses.

A periodic solution of Eq. (17) has eighteen Floquet multipliers and, as the system is Hamiltonian, they appear in pairs $(\psi, 1/\psi)$. Using Proposition 12 of [Muñoz-Almaraz *et al.*, 2002] one can show that the presence of the seven independent conserved quantities implies that at least 14 of these multipliers are located at 1 on the unit circle if the angular momentum $\mathbf{L}$ is zero, and at least 12 if $\mathbf{L} \neq 0$. (The linear momentum $\mathbf{P}$ is always zero along a periodic orbit.) To study the stability and bifurcations of periodic solutions of Eq. (17), one has to monitor the behavior of the remaining "non-trivial" multipliers. For the figure-8 orbit we have $\mathbf{L} = 0$, so that there are four nontrivial multipliers, whose values are given by $\psi = \exp(\pm 2\pi i \nu_j)$, with $\nu_1 = 0.008422$, $\nu_2 = 0.298092$. The smallness of ν_1 indicates that the corresponding multipliers are very close to a double $+1$ situation. Indeed, the numerical results in Sec. 4.2 show that there is a bifurcation point as well as a fold near the figure-8 orbit.

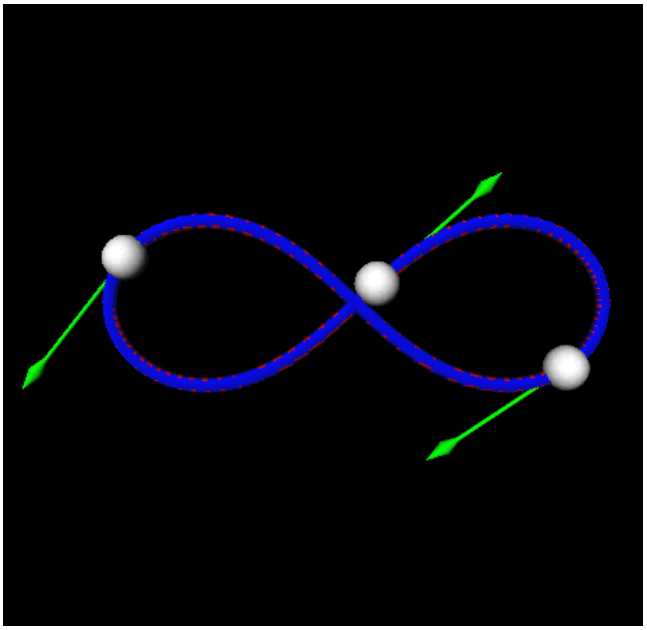

Figure 15: The planar figure-8 orbit [Chenciner & Montgomery, 2000], [Simó, 2000].

Simó discovered hundreds of other single-curve planar periodic solutions for the 3-body problem [Simó, 2002], and many more for the case of n bodies, with n as high as 799 ! (see [Simó, 2000]). Simó called these solutions "choreographies"; the defining property being that all bodies follow a single closed curve in phase space with a fixed delay. From a historical point of view, the solution of Lagrange in 1772 may be considered as the first "choreography", and it has taken more than two hundred years for other choreographies to be found!

4.1 Computational formulation

As in Sec. 2.2, we rewrite Eq. (17) as a first order system with scaled time variable t, so that the unknown period T appears explicitly. We also supplement the equations with appropriate unfolding terms, applying the procedure outlined in Sec. 2.4, generalized to the current situation of seven conserved quantities. In [Muñoz-Almaraz *et al.*, 2002] it is shown that the continuation theorem of Sec. 2.1 can be extended, under certain nondegeneracy conditions, to the case of k linearly independent conserved quantities ($k \geq 1$). If H is the Hamiltonian, and if $\mathbf{P} \equiv (P_x, P_y, P_z)$ (the linear momentum vector) and $\mathbf{L} \equiv (L_x, L_y, L_z)$ (the angular momentum vector) are the additional six conserved quantities, then the resulting system has the form

$$\mathbf{u}' = T\ J\ \nabla H + \alpha \nabla H + \beta_1 \nabla P_x + \beta_2 \nabla P_y + \beta_3 \nabla P_z + \gamma_1 \nabla L_x + \gamma_2 \nabla L_y + \gamma_3 \nabla L_z, \qquad (18)$$

where $\mathbf{u}(t) \equiv (\mathbf{x}, \mathbf{v}) \in \mathbb{R}^{18}$ is the state vector, containing nine spatial coordinates and nine velocities, and where

$$J \equiv \begin{pmatrix} O & I \\ -I & 0 \end{pmatrix}$$

is the standard symplectic matrix, with I denoting the $9-$dimensional identity matrix. The unfolding parameters α, and β_i, γ_i, $(i = 1, 2, 3)$, which are treated as unknowns in the solution procedure, are zero at periodic solutions.

In full detail, the system (18) can be written as

$$\mathbf{x}_1' = T\mathbf{v}_1 + m_1 G(\mathbf{v}_1, \lambda) \ ,$$

$$\mathbf{x}_2' = T\mathbf{v}_2 + m_2 G(\mathbf{v}_2, \lambda) \ ,$$

$$\mathbf{x}_3' = T\mathbf{v}_3 + m_3 G(\mathbf{v}_3, \lambda) \ ,$$

$$\begin{aligned}
\mathbf{v}_1' &= -T\{m_2 \frac{\mathbf{x}_1 - \mathbf{x}_2}{|\mathbf{x}_1 - \mathbf{x}_2|^3} + m_3 \frac{\mathbf{x}_1 - \mathbf{x}_3}{|\mathbf{x}_1 - \mathbf{x}_3|^3}\} + m_1 N(\mathbf{x}_1, \mathbf{v}_1, \lambda), \\
\mathbf{v}_2' &= -T\{m_1 \frac{\mathbf{x}_2 - \mathbf{x}_1}{|\mathbf{x}_1 - \mathbf{x}_2|^3} + m_3 \frac{\mathbf{x}_2 - \mathbf{x}_3}{|\mathbf{x}_2 - \mathbf{x}_3|^3}\} + m_2 N(\mathbf{x}_2, \mathbf{v}_2, \lambda), \\
\mathbf{v}_3' &= -T\{m_2 \frac{\mathbf{x}_3 - \mathbf{x}_2}{|\mathbf{x}_3 - \mathbf{x}_2|^3} + m_1 \frac{\mathbf{x}_3 - \mathbf{x}_1}{|\mathbf{x}_1 - \mathbf{x}_3|^3}\} + m_3 N(\mathbf{x}_3, \mathbf{v}_3, \lambda),
\end{aligned} \tag{19}$$

where the unfolding terms G and N are given by

$$\begin{aligned}
G(\mathbf{v}, \lambda) &= \gamma_1 \begin{pmatrix} 0 \\ v_z \\ -v_y \end{pmatrix} + \gamma_2 \begin{pmatrix} -v_z \\ 0 \\ v_x \end{pmatrix} + \gamma_3 \begin{pmatrix} v_y \\ -v_x \\ 0 \end{pmatrix} \ , \\
N(\mathbf{x}, \mathbf{v}, \lambda) &= \alpha \mathbf{v} + \begin{pmatrix} \beta_1 \\ \beta_2 \\ \beta_3 \end{pmatrix} + \gamma_1 \begin{pmatrix} 0 \\ -z \\ y \end{pmatrix} + \gamma_2 \begin{pmatrix} z \\ 0 \\ -x \end{pmatrix} + \gamma_3 \begin{pmatrix} -y \\ x \\ 0 \end{pmatrix} \ ,
\end{aligned} \tag{20}$$

with

$$\lambda \equiv (\alpha, \beta_1, \beta_2, \beta_3, \gamma_1, \gamma_2, \gamma_3) \ , \qquad \lambda \in \mathbb{R}^7 \ .$$

Equation (18) is supplemented with the periodicity boundary conditions

$$\begin{aligned}
&\mathbf{x}_1(0) - \mathbf{x}_1(1) = 0, \qquad \mathbf{x}_2(0) - \mathbf{x}_2(1) = 0, \qquad \mathbf{x}_3(0) - \mathbf{x}_3(1) = 0 \ , \\
&\mathbf{v}_1(0) - \mathbf{v}_1(1) = 0, \qquad \mathbf{v}_2(0) - \mathbf{v}_2(1) = 0, \qquad \mathbf{v}_3(0) - \mathbf{v}_3(1) = 0 \ .
\end{aligned} \tag{21}$$

Even with fixed masses m_i, $(i = 1, 2, 3)$, a solution of Eq. (19) is not unique, due to the freedom of phase-shift, translation, and rotation, and the scaling invariance $\mathbf{x} \to c\mathbf{x}$, $\mathbf{v} \to c^{-\frac{1}{2}}\mathbf{v}$, $T \to c^{\frac{3}{2}}T$. As shown in [Muñoz-Almaraz *et al.*, 2002] (see, in particular, Theorem 13 and the discussion following that theorem), the scaling invariance can be removed by simply fixing the period. In our calculations we have fixed the period at 2π. Furthermore, following the theory in [Muñoz-Almaraz *et al.*, 2002], the remaining seven invariances can be removed by adding appropriate additional boundary constraints. To be precise, let $\hat{\mathbf{u}}(t) \equiv (\hat{\mathbf{x}}(t), \hat{\mathbf{v}}(t))$ denote a reference periodic solution; as in Sec. 2 the reference solution is typically the preceding solution in the continuation process. The additional boundary conditions are then given by

$$
\begin{aligned}
(\mathbf{u}(0)-\hat{\mathbf{u}}(0))^* J\nabla H(\hat{\mathbf{u}}(0)) &\equiv (\mathbf{u}(0)-\hat{\mathbf{u}}(0))^*\hat{\mathbf{u}}'(0) = 0\ , \\
(\mathbf{u}(0)-\hat{\mathbf{u}}(0))^* J\nabla P_x(\hat{\mathbf{u}}(0)) &\equiv \sum_{i=1}^{3} m_i(x_i-\hat{x}_i) = 0\ , \\
(\mathbf{u}(0)-\hat{\mathbf{u}}(0))^* J\nabla P_y(\hat{\mathbf{u}}(0)) &\equiv \sum_{i=1}^{3} m_i(y_i-\hat{y}_i) = 0\ , \\
(\mathbf{u}(0)-\hat{\mathbf{u}}(0))^* J\nabla P_z(\hat{\mathbf{u}}(0)) &\equiv \sum_{i=1}^{3} m_i(z_i-\hat{z}_i) = 0\ , \\
(\mathbf{u}(0)-\hat{\mathbf{u}}(0))^* J\nabla L_x(\hat{\mathbf{u}}(0)) &\equiv \sum_{i=1}^{3} m_i\left[\hat{y}_i z_i+\dot{\hat{y}}_i\dot{z}_i-\hat{z}_i y_i-\dot{\hat{z}}_i\dot{y}_i\right] = 0\ , \\
(\mathbf{u}(0)-\hat{\mathbf{u}}(0))^* J\nabla L_y(\hat{\mathbf{u}}(0)) &\equiv \sum_{i=1}^{3} m_i\left[\hat{z}_i x_i+\dot{\hat{z}}_i\dot{x}_i-\hat{x}_i z_i-\dot{\hat{x}}_i\dot{z}_i\right] = 0\ , \\
(\mathbf{u}(0)-\hat{\mathbf{u}}(0))^* J\nabla L_z(\hat{\mathbf{u}}(0)) &\equiv \sum_{i=1}^{3} m_i\left[\hat{x}_i y_i+\dot{\hat{x}}_i\dot{y}_i-\hat{y}_i x_i-\dot{\hat{y}}_i\dot{x}_i\right] = 0\ .
\end{aligned}
\tag{22}
$$

The computational formulation now consists of Eqs. (19), (21) and (22); that is, 18 first order ODEs, subject to 18 periodicity conditions and 7 additional boundary constraints. The unknowns in each continuation step are the orbit $(\mathbf{x}(\cdot),\mathbf{v}(\cdot))$, the unfolding parameters λ, and one physical parameter. It follows from the theory in [Muñoz-Almaraz *et al.*, 2002] that the unfolding parameters λ vanish along the solution branch, as is also observed in actual numerical computations.

In our calculations, as described in Sec. 4.2 and Sec. 4.3, we use the mass m_1 of Body 1, as the free physical parameter; the remaining two masses have the fixed value 1. Numerical continuation, starting from the figure-8 orbit of Chenciner and Montgomery, then gives rise to a solution branch along which the computed values of the unfolding vector λ are zero, up to numerical precision. We note that one can also keep all masses fixed at value 1, while allowing the period T to be the free physical variable. This calculation gives the family of figure-8 orbits that arises from the scaling law; each solution is just a scaled version of the previous one with exactly the same stability properties.

Calculations have been done using the unfolding term (20) and the extra boundary constraints (22). However, the choice of unfolding terms and corresponding constraints is not unique. One alternative is to supplement the equations with additional integral constraints, rather than boundary conditions. Although the theory in [Muñoz-Almaraz *et al.*, 2002] is based on additional boundary constraints (and unfolding parameters), it is possible to prove similar results based on integral constraints (and unfolding parameters). Specifically, we have done extensive calculations with the integral constraints described below, which basically correspond to integrated versions of the boundary constraints in Eq. (22).

The phase can be fixed by the integral constraint ($5a_3$), which, leaving out the $\mathbf{v}$-component, can here be written as

$$
\sum_{i=1}^{3}\int_0^1 \langle \mathbf{x}_i(\tau),\hat{\mathbf{x}}_i'(\tau)\rangle\ d\tau = 0\ . \tag{23}
$$

Note that Eq. (23) is a necessary condition for the relative phase-drift measure

$$\sum_{i=1}^{3} \int_0^1 ||\mathbf{x}_i(\tau+\sigma) - \hat{\mathbf{x}}_i(\tau)||^2 \, d\tau \ ,$$

to be minimized over $\sigma \in \mathbb{R}$ [Doedel *et al.*, 1991c]. As before, the reference solution $(\hat{\mathbf{x}}(\cdot), \hat{\mathbf{v}}(\cdot))$ is normally the preceding solution computed in the continuation process. Thus, as already mentioned in Sec. 2.2, the integral phase condition (23) has the effect of aligning the current solution as much as possible with the previous solution. Often this allows much bigger continuation steps to be taken along a solution branch.

The translation freedom can be removed by requiring

$$\sum_{i=1}^{3} m_i \int_0^1 [\mathbf{x}_i(\tau) - \hat{\mathbf{x}}_i(\tau)] \, d\tau = 0 \ . \tag{24}$$

Note that (24) consists of three scalar integral constraints, which correspond to the necessary conditions for minimizing the relative translation measure

$$\sum_{i=1}^{3} m_i \int_0^1 ||\mathbf{x}_i(\tau) + \mathbf{s} - \hat{\mathbf{x}}_i(\tau)||^2 \, d\tau \ ,$$

over $\mathbf{s} \in \mathbb{R}^3$.

The rotational freedom can be eliminated by adding the integral constraints

$$\sum_{i=1}^{3} m_i \int_0^1 \mathbf{x}_i(\tau) \times \hat{\mathbf{x}}_i(\tau) \, d\tau = 0 \ , \tag{25}$$

where we have left out the $\mathbf{v}$-component. Equation (25) expresses the fact that the $\mathbf{x}_i$ are "on the average" parallel to the $\hat{\mathbf{x}}_i$. Written individually, these constraints are given by the equations

$$\begin{aligned}
&\text{a)} \quad \sum_{i=1}^{3} m_i \int_0^1 \{\hat{z}_i(\tau) y_i(\tau) - \hat{y}_i(\tau) z_i(\tau)\} \, d\tau = 0 \ , \\
&\text{b)} \quad \sum_{i=1}^{3} m_i \int_0^1 \{\hat{x}_i(\tau) z_i(\tau) - \hat{z}_i(\tau) x_i(\tau)\} \, d\tau = 0 \ , \\
&\text{c)} \quad \sum_{i=1}^{3} m_i \int_0^1 \{\hat{y}_i(\tau) x_i(\tau) - \hat{x}_i(\tau) y_i(\tau)\} \, d\tau = 0 \ ,
\end{aligned} \tag{26}$$

which fix rotation about the x, y, and z axis, respectively, relative to the reference orbit $\hat{\mathbf{x}}(\cdot)$.

The integral phase constraint (23) regularizes the continuation whenever the Poincaré point-wise phase condition does [Doedel *et al.*, 1991c]. Similar results hold for the integral versus boundary conditions for fixing the translation and rotation invariances. The integral phase condition often drastically reduces the number of steps required to trace out a solution branch, especially near homoclinic orbits and near simple collisions. Properly chosen integral constraints for fixing translation and rotation have similar advantages over corresponding boundary constraints.

For periodic orbits near heteroclinic orbits, or near multiple collisions, the advantage of integral constraints over pointwise constraints is less clear. In this case there are multiple small regions (in scaled time) where solutions vary rapidly, and these regions may necessarily move relative to each other during continuation. This renders impossible the desirable property of having all mesh point accumulations in fixed locations, as was the case, for example, in Fig. 2_{bottom}. Indeed, such calculations typically require very small continuation steps.

4.2 Local continuation of the figure-8 orbit

The local continuation of the Chenciner-Montgomery figure-8 solution, as the value of one of the masses is allowed to vary on a very small scale, is represented in Fig. 16_{bottom}, where the L_2 norm of the solution is plotted versus the mass m_1. Solution 1 is the figure-8 orbit, and the solid curve segment containing Solution 1 corresponds to the portion of the solution branch where solutions are elliptically stable. The non-unity multipliers of the figure-8 solution are given by $\psi_j = \exp(\pm 2\pi i \nu_j)$, with $\nu_1 = 0.008422$, and $\nu_2 = 0.298092$, which is in agreement with Simó's results. All solutions represented in Fig. 16_{bottom} have angular momentum $\mathbf{L} = 0$, and, as discussed earlier, they therefore have four nontrivial multipliers.

For increasing m_1 the family reaches a *fold bifurcation*, or *limit point* (LP), where the branch turns back towards lower values of m_1. At the fold the solution loses stability and becomes hyperbolic. Continuing past the fold, one arrives at another periodic orbit for which all masses are equal to 1, namely, Solution 1a. (The "straight line" solution branch that appears to pass through Solution 1a will be described at the end of this section.) The unstable solution 1a is homotopic to the figure-8 solution, as one can continuously deform one orbit into the other. However, Solution 1a is hyperbolic and not a choreography; the three bodies follow slightly different figure-8 paths. In fact, Solution 1 is the only choreography on the branch.

Remarkably, within the precision of our calculations, the action integral of Solution 1a is identical to that of the figure-8 orbit. Recall that if $\mathbf{x}(t)$ is a trajectory that goes from $\mathbf{x}_1 = \mathbf{x}(t_1)$ to $\mathbf{x}_2 = \mathbf{x}(t_2)$, then the *action*, usually denoted by S, is the integral of the Lagrangian over time from t_1 to t_2, where the Lagrangian $\mathcal{L}$ is the difference between the kinetic energy K and the potential energy V :

$$S = \int_{t_1}^{t_2} \mathcal{L}(t)\, dt = \int_{t_1}^{t_2} K(\mathbf{x}'(t)) - V(\mathbf{x}(t))\, dt \ .$$

The action depends therefore on the initial and final time and on the trajectory. The Principle of Least Action states that the true trajectory, *i.e.*, the one that satisfies Newton's laws, is the minimizer of the action. The problem is to find the minimizer among all possible trajectories, *i.e.*, minimizing the action is an alternative to applying Newton's Laws. (For an excellent exposition see Lecture 19 in Volume II of the Feynman Lectures on Physics [Feynman *et al.*, 1964].) Note that our solution algorithm, which uses a boundary value approach coupled to a continuation algorithm, does not use the minimizing property of the action integral for orbits. We can, of course, easily compute the action integral as a by-product of our numerical scheme. For the figure-8 orbit its value is found to be $S = 24.37197$.

There has been some question about the stability of the actual minimizer of the action. Apparently it is not clear whether the minimizer is elliptic. Minimizing orbits are unstable in Hamiltonian systems with two degrees of freedom [Birkhoff, 1927]. However, for higher-dimensional systems there are counter-examples to this statement. Thus it is possible that

there exists a less symmetric solution that is the actual minimizer of the action for the equal-mass three-body problem. From the variational view point, if one enlarges the space of arcs over which the action is minimized, then obviously the action will not increase. The actual minimizing orbit would be (i) in the same homotopy class as the figure-8 orbit, and (ii) no longer a choreography. Note that Solution 1a in Fig. $16_{\rm bottom}$ satisfies these two properties. However, we cannot explain why the action integral of Solution 1a is, to numerical precision, identical to that of the figure-8 orbit. Two other well-known periodic solutions of the equal-mass three-body problem, with normalized period 2π, have lower values of the action; namely, the Lagrange solution $S_L = 3\pi 3^{2/3} \approx 19.60436$, which is stable, and the Euler solution $S_E = 3\pi 5^{2/3}/2^{1/3} \approx 21.87299$, which is unstable.

Figure 17 shows Solution 1 and Solution 1a in projected phase space. The behavior of the complex conjugate pair of Floquet multipliers closest to 1, as a function of the mass m_1, is shown in Fig. 18. The upper panel is the logarithm of the modulus of this multiplier and the lower panel is its principal argument. (The second complex conjugate pair, which is not shown, remains complex in the parameter range under consideration, it varies very little, and its argument is outside the scale of Fig. $18_{\rm bottom}$.) The elliptic region is restricted to the m_1-interval where the multipliers have non-zero argument. Examining the non-zero values of the logarithm of the modulus, one can identify two bifurcations in this diagram, namely, the fold bifurcation mentioned above, and a pitch-fork bifurcation at a value of m_1 just below 1.

The pitch-fork bifurcation can be seen in Fig. $16_{\rm bottom}$, where its two legs coincide due to our choice of vertical axis. There are four distinct solutions having $m_1 = 1$ in this diagram, namely, Solution 1 (the figure-8 orbit), Solution 1a, and the solutions at $m_1 = 1$ on the two legs of the pitch-fork branch. In the bifurcation diagram the pitch-fork branch appears to reconnect to the primary branch at Solution 1a. However, this is an artifact of our choice of vertical axis and not an actual bifurcation point. Further continuation of the two legs of the pitch-fork branch for $m_1 > 1$ leads to collision orbits that we do not discuss here.

4.3 Global continuation of the figure-8 orbit.

We now describe some computational results for the continuation of the figure-8 orbit as the mass of Body 1 is allowed to vary on a larger scale, namely, between 1 and 0. As discussed above, Fig. $16_{\rm bottom}$ shows the local continuation of the figure-8 orbit, for values of m_1 very close to 1. Solution 1 and Solution 1a lie on the same branch; they are connected via a fold. It is of interest to continue these two solutions to smaller values of m_1. The result of this continuation is shown in Fig. $16_{\rm top}$. The two lower diagrams correspond to consecutive blow-ups of the top diagram near $m_1 = 1$.

Solutions at labeled points in Fig. 16 are shown in separate Figures: Solution 1 is the figure-8 orbit of Chenciner and Montgomery, which appears in Fig. 15 and Fig. 17, while Solutions 2-7 are shown in Fig. 19.

The branch containing Solutions 1-4 consists entirely of planar periodic orbits with zero angular momentum. Solution 2 marks a bifurcation point, where a solution branch consisting of non-planar periodic orbits with non-zero angular momentum bifurcates. We have located several more bifurcation points, for example, Solution 5, but to keep the presentation simple we only show the branch that bifurcates from Solution 2.

Continuation of the figure-8 orbit, *i.e.*, Solution 1, in the direction of decreasing m_1 leads to a collision orbit near Solution 3, where the smaller mass, *i.e.*, Body 1, collides with the larger bodies. There are four such near-collisions along Solution 3. Continuation of the

figure-8 orbit in opposite direction, via the fold and via Solution 1a in Fig. 16_{bottom} leads to another type of collision orbit near Solution 4, where the two larger bodies collide with each other. There are two such near-collisions along Solution 4, while the smaller body completes a near-horizontal motion.

Solution 5 marks a bifurcation point on the branch of non-planar solutions; the branch that bifurcates at this point is not shown. Solutions 6 and 7 are also on the branch of non-planar solutions. Note that $m_1 = 0$ at Solution 7; therefore it is also a solution of the restricted 3-body problem. (Note, however, that the mass-ratio parameter μ is equal to 0.5 here, while in Sec. 3 we had $\mu = 0.01215$, corresponding to the Earth-Moon system.) Our computations therefore establish a homotopy from the figure-8 orbit of Chenciner and Montgomery to a periodic solution of the restricted 3-body problem. The complete homotopy path requires branch switching at the bifurcation point denoted as Solution 2. More extensive computations, that we do not report here, establish the existence of further homotopy paths from the figure-8 orbit to other solutions of the restricted 3-body problem. All these paths pass through Solution 2 and switch to the branch of 3D orbits there. We have not found a homotopy from the figure-8 solution to a solution of the restricted 3-body problem, where the orbits remain planar along the entire homotopy path.

As mentioned before, the figure-8 orbit is elliptically stable, and this stability is preserved in a very small neighborhood of m_1-values. However, most solutions determined in the continuation process are unstable (hyperbolic). Our computational scheme does not distinguish between stable and unstable periodic solutions; it can compute both solution types equally well. In real astronomical observations, on the other hand, only stable periodic orbits are observed. By carefully monitoring the Floquet multipliers along solution branches and by following more bifurcating branches, we have located other regions along solution branches where elliptically stable periodic orbits exist. However, some of these regions are very small, so that the likelihood of encountering such orbits in physical observations is exceedingly small.

5 Conclusion

We have shown how standard numerical continuation and bifurcation methods can be used to compute families of periodic orbits in conservative systems and determine their bifurcations. We have applied the computational techniques to the restricted 3-body problem and to the general 3-body problem, and we have presented a limited collection of numerical results that illustrate the power and ease of application of the methods. Systematic application of the techniques can lead to new discoveries that increase our understanding of the global periodic solution structure of these problems.

Future work on the restricted 3-body problem includes a complete classification of the periodic solution branches that emanate from all five libration points, and their subsequent bifurcations, for all values of the mass-ratio parameter μ. Future work on the general n-body problem includes the extension of the methods in order to deal with the continuation of periodic solutions from the Euler solution and the Lagrange solution. An interesting conjecture is the existence of a homotopy from the figure-8 solution of Chenciner and Montgomery to the 3-body Lagrange solution. In fact, it was this conjecture of Professor J. B. Keller that motivated us to design the current computational scheme for the continuation of periodic solutions of the 3-body problem. The conjecture remains open, however.

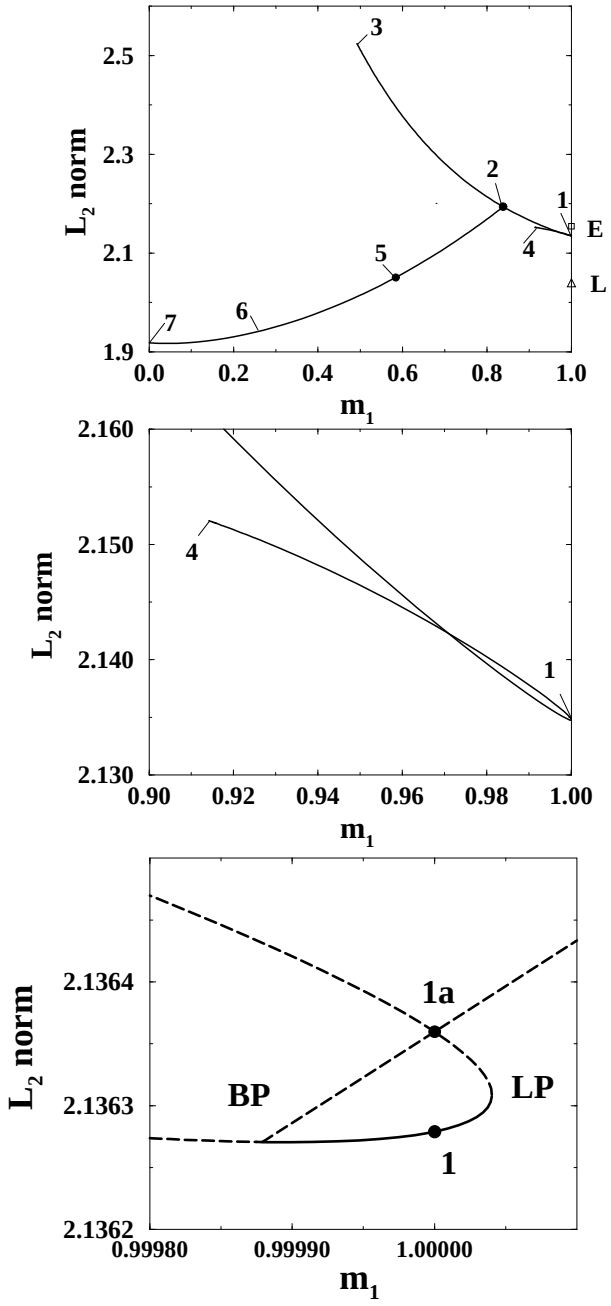

Figure 16: Continuation of the figure-8 orbit. The solution L_2 norm is plotted versus the mass of Body 1. The lower Figures are successive blow-ups of the top Figure. Solutions at labeled points appear in Figs. 15, 17, and 19. *Top*: The primary branch of planar solutions obtained by continuing the figure-8 orbit (Solution 1), and a branch of non-planar solutions that bifurcates at Solution 2. The end points of the primary branch, Solutions 3 and 4, are near collision orbits. Solution 5 is a bifurcation point on the non-planar solution branch; the bifurcating branch is not shown. Solutions 6 and 7 are further non-planar solutions. Solution 7 is also a solution of the restricted 3-body problem. *Center*: A blow-up of the primary solution branch near the figure-8 orbit. Solution 4 is near a collision orbit. *Bottom*: A further blow-up of the primary solution branch near the figure-8 orbit. Solution 1a is another solution at $m_1 = 1$ on the primary branch; however, it is not a choreography (see Fig. 17). LP and BP denote a fold and a pitch-fork bifurcation; at these points the primary solutions lose stability. The bifurcating pitch-fork branch appears to reconnect to the primary branch at Solution 1a; however, this is not an actual bifurcation point.

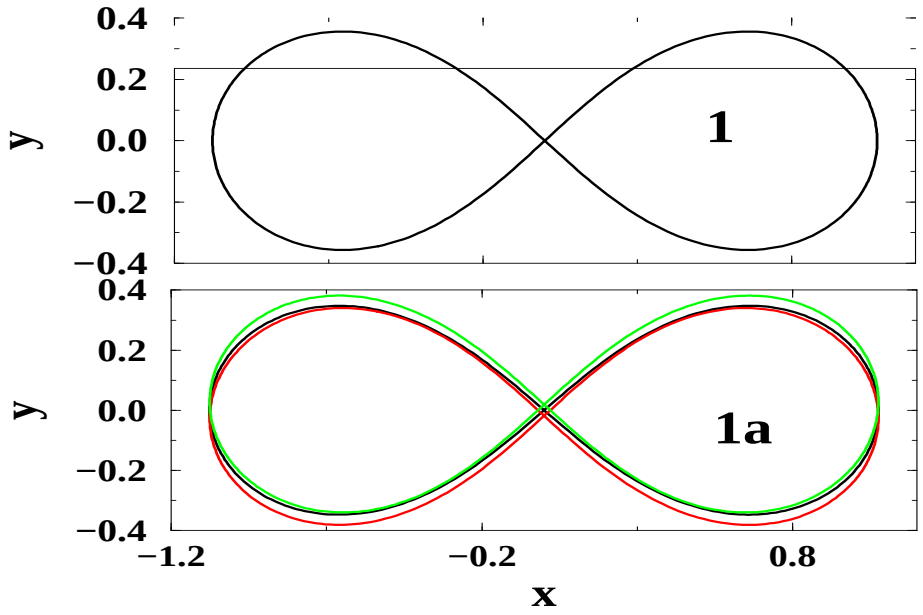

Figure 17: Projected phase-space representation of Solutions 1 and 1a from Fig. 16.

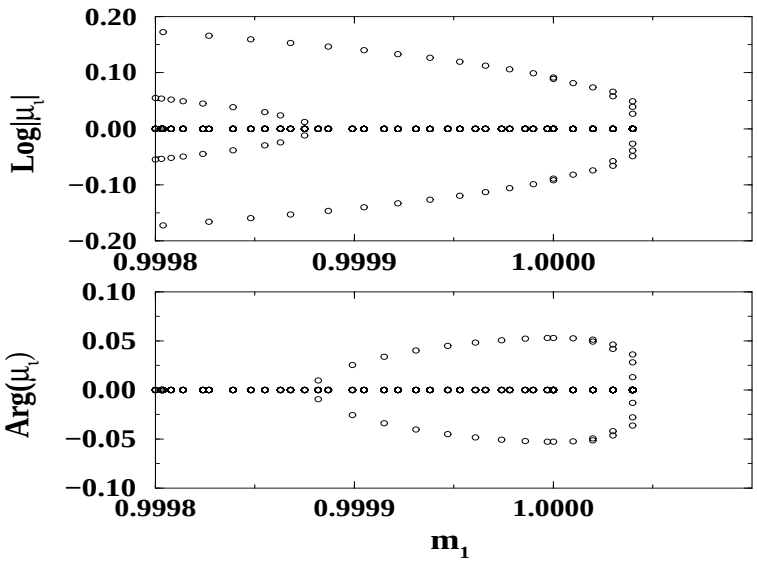

Figure 18: The behavior of the complex conjugate pair of Floquet multipliers that is closest to 1, for the family of orbits that passes through the figure-8 orbit. *Top:* The logarithm of the modulus of the Floquet multipliers. *Bottom:* The principal argument of the Floquet multipliers.

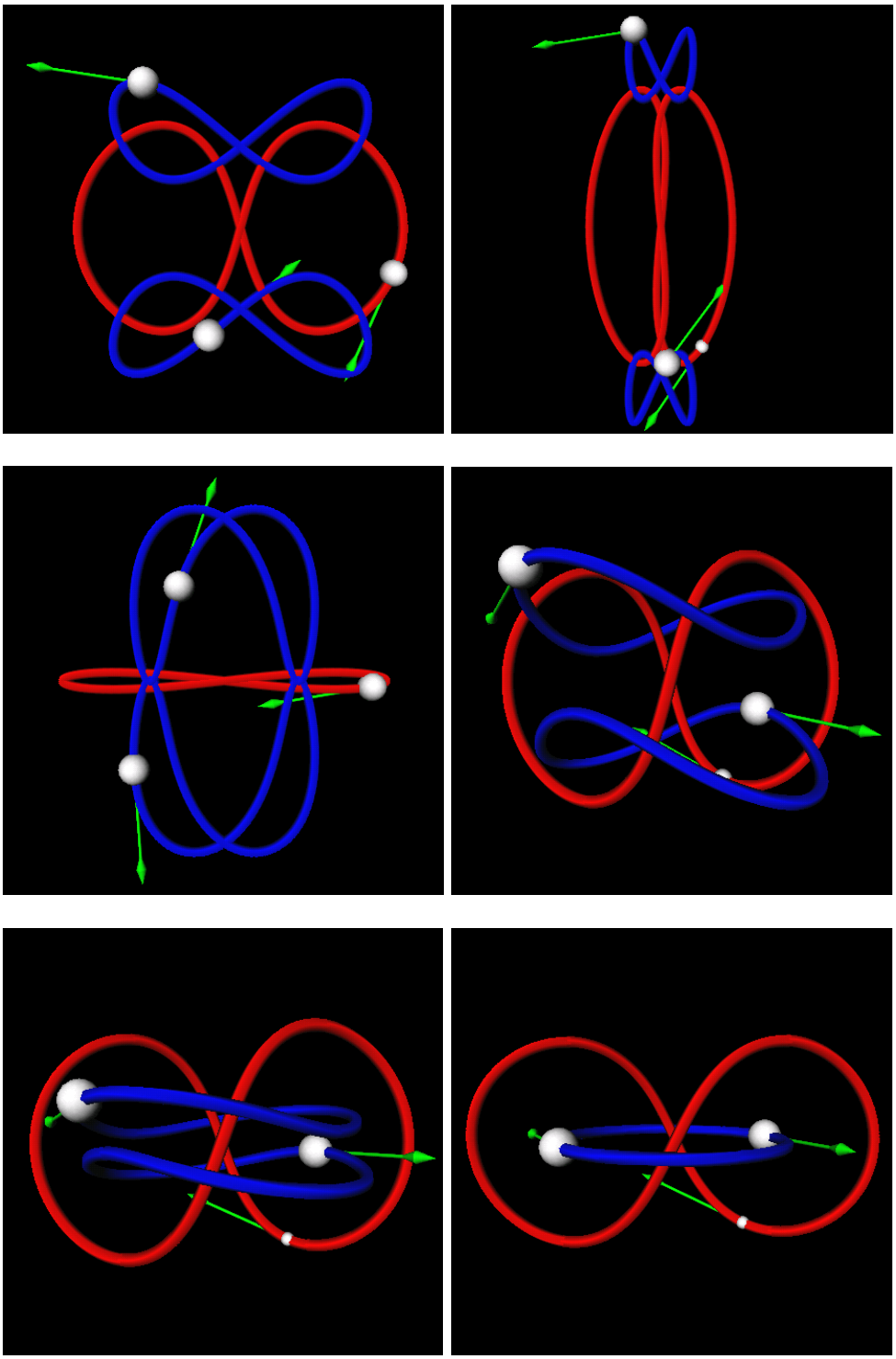

Figure 19: Selected orbits from Fig. 16: *Top left:* Solution 2 (at the bifurcation point to non-planar solutions). *Top right:* Solution 3 (close to small body-large bodies collisions). *Center left:* Solution 4 (near collisions of the large bodies). *Center right:* Solution 5 (a non-planar solution at a bifurcation point). *Bottom left:* Solution 6 (another non-planar solution). *Bottom right:* Solution 7 (a solution of the restricted 3-body problem).

Supplementary Bibliography

A more general and detailed theoretical treatment of our computational methods for conservative systems can be found in [Muñoz-Almaraz *et al.*, 2002]. For related theory see [Vanderbauwhede, 1982], [Meyer, 1973; Schmidt, 1978; Kirchgraber, 1980] and, more recently, [Sepulchre & MacKay, 1997]. For recent papers with alternate numerical approaches for conservative systems see [Jorba, 1999] and [Viswanath, 2001].

We can only give some pointers to the vast literature on the general n-body problem, the CR3BP, and related topics. *Les Méthodes Nouvelles de la Mécanique Céleste* of Poincaré [1899] (English translation [1993]) is a seminal work on the CR3BP which developed fundamental concepts in dynamical systems. Orbital mechanics texts that examine the n-body problem and the CR3BP in particular, include [Roy, 1988] and [Danby, 1992]. Meyer & Hall [1999] considered the n-body problem and the CR3BP from the point of view of Hamiltonian systems theory, while Meyer [1999] focused on periodic solutions. For books on the 3-body problem see [Szebehely, 1967] and [Bruno, 1994], both of which focus on the planar problem, and [Marchal, 1990].

The use of libration points for space missions was already mentioned by Clarke [1947]. The January-March 2001 issue of the Journal of the Astronautical Sciences contains many articles on libration point missions, including several already cited here. Other references on orbits near libration points can be found in [Bray & Goudas, 1967a], [Bray & Goudas, 1967b], [Meer, 1985], and [Gabern & Jorba, 2001]. Corresponding mission design aspects are considered in [Gómez *et al.*, 1991] and [Gómez *et al.*, 1993]. For additional literature on 3D orbits near the libration points see [Goudas, 1963], [Kazantzis, 1978], [Kazantzis, 1979a], [Kazantzis, 1979b], [Robin & Markellos, 1980], and [Jorba & Masdemont, 1999]. Recent results on vertical orbits can be found in [Jorba & Villanueva, 1998], and for collisions see [Simó, 2001a]. Some other relevant papers on the CR3BP include [Michalodimitrakis, 1978], [Kwok, 1980], [Meyer, 1981a], and [Meyer & Schmidt, 2000].

For more papers on the figure-8 orbit see [Chenciner *et al.*, 2001] and [Simó, 2001b]. Further pointers to the general n-body literature include [Broucke, 1978], [Hulkower, 1980], [Gómez & Llibre, 1981], [Montgomery, 1997], and [Stuchi *et al.*, 2000].

Acknowledgments

EJD, RCP, and HBK thank Professor J. B. Keller (Stanford University) for asking us to continue the figure-8 orbit of Chenciner and Montgomery. EJD is indebted to Dr. Neal Hulkower of RAF (Redmond WA) for enjoyable informative conversations and for access to documents stored in his garage. The work of EJD and RCP has been partially supported by NSF grant KDI/NCC SBR-9873173. EJD is also supported by NSERC Canada, Research Grant A4274. DJD thanks R. W. Farquhar and K. C. Howell for introducing him to the fascinating subject of libration point mission design. JGV is indebted to E. Freire, F. J. Muñoz-Almaraz, J. Llibre, R. Montgomery and A. Zevin for helpful discussions. JGV acknowledges funding from NATO (CRG-972260), DGES PB-1152 and PB-0142. The authors thank David Goldstein at the Aerospace Corporation for valuable comments. They also gratefully acknowledge the artistic assistance of Christine Thorn in the preparation of the Figures.

References

Allgower, E. L. & Georg, K. [1996] "Numerical path following," in *Handbook of Numerical Analysis* **5**, eds. Ciarlet, P. G. & Lions, J. L. (North Holland Publishing).

Arenstorf, R. F. [1976] "Some families of periodic solutions in the planar n-body problem," *Celestial Mechanics* **14**, 5–9.

Ascher, U. M., Christiansen, J., & Russell, R. D. [1981] "Collocation software for boundary value ODEs," *ACM Trans. Math. Software* **7**, 209–222.

Ascher, U. M., Mattheij, R. M. M., & Russell, R. D. [1995] *Numerical Solution of Boundary Value Problems for Ordinary Differential Equations* (SIAM).

Ascher, U. M. & Petzold, L. R. [1998] *Computer Methods for ODEs and DAEs* (SIAM).

Ascher, U. M. & Spiteri, R. J. [1995] "Collocation software for boundary value differential-algebraic equations," *SIAM J. Sci. Comput.* **15**, 938–952.

Barden, B. T. & Howell, K. C. [1998] "Fundamental motions near collinear libration points and their transitions," *J. Astronautical Sciences* **46**(4), 361–378.

Beyn, W.-J., Champneys, A., Doedel, E. J., Govaerts, W., Sandstede, B., & Kuznetov, Y. A. [2002] "Numerical continuation and computation of normal forms," in *Handbook of Dynamical Systems* **2**, ed. Fiedler, B. (Elsevier Science) pp. 149–219.

Birkhoff, G. D. [1927] *Dynamical Systems* (Amer. Math. Soc.)

Bray, T. A. & Goudas, C. L. [1967a] "Doubly symmetric orbits about the collinear Lagrangian points," *The Astronomical Journal* **72**(2), 202–213.

Bray, T. A. & Goudas, C. L. [1967b] "Three-dimensional periodic oscillations about L1, L2 and L3," in *Advances in Astronomy and Astrophysics* **5**, ed. Kopal, Z. (Academic Press) pp. 71–130.

Breakwell, J. V. & Brown, J. V. [1979] "The Halo family of 3-dimensional periodic orbits in the Earth-Moon restricted 3-body problem," *Celestial Mechanics* **20**, 389–404.

Broucke, R. [1978] "On the isosceles triangle configuration in the planar general three-body problem," *Astron. Astrophys.* **73**, 303–313.

Bruno, A. D. [1994] *The Restricted 3-Body Problem: Plane Periodic Orbits* (De Gruyter, Berlin, New York).

Bruno, A. D. [2001] "Families of periodic solutions of the Beletskii equation," Technical report, Keldysh Institute of Applied Mathematics of RAS, Moscow.

Chenciner, A., Gerver, J., Montgomery, R., & Simó, C. [2001] "Simple choreographic motions of n bodies: A preliminary study," Technical report, Departament de Matemàtica i Anàlisi, Universitat de Barcelona.

Chenciner, A. & Montgomery, R. [2000] "A remarkable periodic solution of the three body problem in the case of equal masses," *Annals of Mathematics* **152**, 881–901.

Clarke, A. C. [1945] "Extra-terrestial relays," *Wireless world*, pp. 305–308. Reprinted in *Ascent to Orbit: A Scientific Autobiography*, A.C. Clarke (Wiley, 1984).

Clarke, A. C. [1947] "Stationary orbits," *J. British Astronomical Association*, pp. 232–237. Reprinted in *Ascent to Orbit: A Scientific Autobiography*, A.C. Clarke (Wiley, 1984).

Danby, J. M. A. [1992] *Fundamentals of Celestial Mechanics* (Willmann-Bell).

Davoust, E. & Broucke, R. [1982] "On the manifold of periodic orbits in the planar general three-body problem with equal masses," *Astron. Astrophys.* **112**, 305–320.

de Boor, C. & Swartz, B. [1973] "Collocation at Gaussian points," *SIAM J. Numer. Anal.* **10**, 582–606.

Deprit, A. & Henrard, J. [1968] "A manifold of periodic orbits," in *Advances in Astronomy and Astrophysics*, ed. Kopal, Z. (Academic Press) pp. 1–124.

Deprit, A. & Henrard, J. [1969] "Construction of orbits asymptotic to a periodic orbit," *Astron. J.* **74**, 308–316.

Deprit, A. & Henrard, J. [1970] The "Trojan manifold - Survey and conjectures," in *Periodic Orbits, Stability and Resonances*, ed. Giacaglia, G. E. O. (D. Reidel Publishing Co., Dordrecht-Holland) pp. 1–18.

Doedel, E. J. [1981] "AUTO, a program for the automatic bifurcation analysis of autonomous systems," *Congr. Numer.* **30**, 265–384.

Doedel, E. J. [1997] "Nonlinear numerics," *Int. J. Bifurcation and Chaos* **7**(9), 2127–2143.

Doedel, E. J., Aronson, D. G., & Othmer, H. G. [1991a] "The dynamics of coupled current-biased Josephson junctions II," *Int. J. Bifurcation and Chaos* **1**(1), 51–66.

Doedel, E. J., Champneys, A. R., Fairgrieve, T. F., Kuznetsov, Y. A., Sandstede, B., & Wang, X. J. [1997] "Continuation and bifurcation software for ordinary differential equations," Available via http://cmvl.cs.concordia.ca.

Doedel, E. J., Jepson, A. D., & Keller, H. B. [1984] "Numerical methods for Hopf bifurcation and continuation of periodic solution paths," in *Computing Methods in Applied Sciences and Engineering VI*, eds. Glowinski, R. & Lions, J. L. (North Holland, Amsterdam) pp. 127–136.

Doedel, E. J., Keller, H. B., & Kernévez, J. P. [1991b] "Numerical analysis and control of bifurcation problems: I," *Int. J. Bifurcation and Chaos* **1**(3), 493–520.

Doedel, E. J., Keller, H. B., & Kernévez, J. P. [1991c] "Numerical analysis and control of bifurcation problems: II," *Int. J. Bifurcation and Chaos* **1**(4), 745–772.

Doedel, E. J. & Paffenroth, R. C. [2001] "The AUTO2000 command line user interface," in *Proceedings of the 9th International Python Conference, Long Beach*, 233–241.

Doedel, E. J., Paffenroth, R. C., Champneys, A. R., Fairgrieve, T. F., Kuznetsov, Y. A., Oldeman, B. E., Sandstede, B., & Wang, X. J. [2000] "AUTO2000: Continuation and bifurcation software for ordinary differential equations," Available via http://cmvl.cs.concordia.ca.

Dunham, D. W. & Roberts, C. E. [2001] "Stationkeeping techniques for libration-point satellites," *J. Astronautical Sciences* **49**(1), 127–144.

Fairgrieve, T. F. & Jepson, A. D. [1991] "O. K. Floquet multipliers," *SIAM J. Numer. Anal.* **28**(5), 1446–1462.

Farquhar, R. [1968] *The Control and Use of Libration-Point Satellites*, PhD thesis, Department of Aeronautics and Astronautics, Stanford University.

Farquhar, R. W. [2001] "The flight of ISEE-3/ICE: Origins, mission history and a legacy," *J. Astronautical Sciences* **49**(1), 23–73.

Farquhar, R. W. & Dunham, D. W. [1990] "Use of libration points for space observatories," in *Observatories in Earth Orbit and Beyond* (Kluwer Academic Publishers) pp. 391–395.

Farquhar, R. W. & Kamel, A. K. [1973] "Quasi-periodic orbits about the translunar libration

point," *Celestial Mechanics* **7**, 458–473.

Felici, F., Hechler, M., & Vanderbussche, F. [2001] "The ESA astronomy missions at L2: FIRST and Planck," *J. Astronautical Sciences* **49**(1), 185–196.

Feynman, R. P., Leighton, R. B., & Sands, M. [1964] *The Feynman Lectures on Physics* (Addison-Wesley).

Folta, D., Cooley, S., & Howell, K. [2001a] "Trajectory design strategies for the NGST L2 libration point mission," in *AAS/AIAA Space Flight Mechanics Meeting*, AAS 01-205.

Folta, D. & Richon, K. [1998] "Libration orbit mission design at L2: A MAP and NGST perspective," in *AIAA/AAS Astrodynamics Specialist Conference*, AIAA 98-4469.

Folta, D., Young, C., & Ross, A. [2001b] "Unique non-Keplerian orbit vantage locations for Sun-Earth connections and Earth Science Vision roadmaps," in *NASA Goddard Flight Dynamics Symposium*.

Gabern, F. & Jorba, A. [2001] "A restricted four-body model for the dynamics near the Lagrangian points of the Sun-Jupiter system," *Discrete and Continuous Dynamical Systems-Series B*, **1**(2), 143–182.

Gómez, G., Jorba, A., Masdemont, J., & Simó, C. [1991] "Moon's influence on the transfer from the Earth to a Halo orbit around L1," in *Predictability, Stability, and Chaos in N-Body Dynamical Systems*, ed. Roy, A. E. (Plenum Press) pp. 283–290.

Gómez, G., Jorba, A., Masdemont, J., & Simó, C. [1993] "Study of the transfer from the Earth to a Halo orbit around the equilibrium point L1," *Celestial Mechanics and Dynamical Astronomy* **56**, 541–562.

Gómez, G., Koon, K. S., Lo, M. W., Marsden, J. E., Masdemont, J., & Ross, S. D. [2001a] "Invariant manifolds, the spatial three-body problem and space mission design," in *AAS/AIAA Astrodynamics Specialist Conference*, AAS 01-301.

Gómez, G. & Llibre, J. [1981] "A note on a conjecture by Poincaré," *Celestial Mechanics* **24**(4), 335–343.

Gómez, G., Llibre, J., Martínez, R., & Simó, C. [2001b] *Dynamics and Mission Design Near Libration Points, Vol. II: Fundamentals: The Case of Triangular Libration Points* **3** (World Scientific).

Gómez, G., Llibre, J., Martínez, R., & Simó, C. [2001c] *Dynamics and Mission Design Near Libration Points, Volume I: Fundamentals : The Case of Collinear Libration Points* **2** (World Scientific).

Gómez, G., Lo, M. W., Masdemont, J., & Museth, K. [2001d] "Simulation of formation flight near Lagrange points for the TPF mission," in *AAS/AIAA Astrodynamics Specialist Conference*, AAS 01-305.

Gómez, G., Masdemont, J., & Simó, C. [1997] "Lissajous orbits around Halo orbits," in *AAS/AIAA Space Flight Mechanics Meeting*, AAS 97-106.

Gómez, G. & Noguera, M. [1985] "Some manifolds of periodic orbits in the restricted three-body problem," *Celestial Mechanics* **35**, 235–255.

Goudas, C. L. [1963] "Three-dimensional periodic orbits and their stability," *Icarus* **2**, 1–18.

Hadjidemetriou, J. [1975] "The continuation of periodic orbits from the restricted to the general three-body problem," *Celestial Mechanics* **12**, 155–174.

Henderson, M. [2002] "Multiple parameter continuation: Computing implicitly defined k-manifolds," *Int. J. Bifurcation and Chaos* **12**(3), 451–476.

Hénon, M. [1997] *Generating Families in the Restricted Problem* (Springer-Verlag).

Hénon, M. [2001] *Generating Families in the Restricted Problem, II, Quantitative Study of Bifurcations* (Springer-Verlag).

Howell, K. C. [1984] "Three-dimensional, periodic, Halo orbits," *Celestial Mechanics* **32**, 53–71.

Howell, K. C. [2001] "Families of orbits in the vicinity of the collinear libration points," *J. Astronautical Sciences* **49**(1), 107–125.

Howell, K. C., Barden, B. T., & Lo, M. W. [1997] "Applications of dynamical systems theory to trajectory design for a libration point mission," *J. Astronautical Sciences* **45**(2), 161–178.

Howell, K. C. & Campbell, E. T. [1999] "Three-dimensional periodic solutions that bifurcate from Halo families in the circular restricted three-body problem," in *Spaceflight Mechanics*, AAS 99-161.

Howell, K. C. & Farquhar, R. W. [1993] "John Breakwell, the restricted problem, and Halo orbits," *Acta Astronautica* **29**, 485–488.

Hulkower, N. D. [1980] "Central configurations and hyperbolic-elliptic motion in the three-body problem," *Celestial Mechanics* **21**, 37–41.

Ichtiaroglou, S. & Michalodimitrakis, M. [1980] "Three-body problem: The existence of families of three-dimensional periodic orbits," *Astronomy and Astrophysics* **81**, 30–32.

Jepson, A. D. [1981] *Numerical Hopf Bifurcation*, PhD thesis, Applied Mathematics, California Institute of Technology.

Jorba, A. [1999] "A methodology for the numerical computation of normal forms, centre manifolds, and first integrals of Hamiltonian systems," *Experimental Mathematics* **8**(2), 155–195.

Jorba, A. & Masdemont, J. [1999] "Dynamics in the center manifold of the collinear points of the restricted three body problem," *Physica D* **132**, 189–213.

Jorba, A. & Villanueva, J. [1998] "Stability and asymptotic behavior of the vertical family of periodic orbits around L5 of the restricted three body problem," in *Actas del XV CEDYA / V CMA* (Universidad de Vigo) pp. 303–308.

Kazantzis, P. G. [1978] "The structure of periodic solutions in the restricted problem of three-body: Sun-Jupiter case," *Astrophysics and Space Science* **59**, 355–371.

Kazantzis, P. G. [1979a] "Families of three-dimensional axisymmetric periodic orbits in the restricted three-body problem: Sun-Jupiter case," *Astrophysics and Space Science* **61**, 477–486.

Kazantzis, P. G. [1979b] "Families of three-dimensional plane-symmetric periodic orbits in the restricted three-body problem: Sun-Jupiter case," *Astrophysics and Space Science* **61**, 357–367.

Keller, H. B. [1977] "Numerical solution of bifurcation and nonlinear eigenvalue problems," in *Applications of Bifurcation Theory*, ed. Rabinowitz, P. H. (Academic Press) pp. 359–384.

Kirchgraber, U. [1980] "A note on Liapunov's center theorem," *J. Math. Anal. Appl.* **73**, 568–570.

Koon, W. S., Lo, M. W., Marsden, J. E., & Ross, S. D. [1999] "The Genesis trajectory and heteroclinic connections," in *AAS/AIAA Astrodynamics Specialist Conference*, AAS 99-451.

Koon, W. S., Lo, M. W., Marsden, J. E., & Ross, S. D. [2000] "Heteroclinic connections between periodic orbits and resonance transitions in celestial mechanics," *Chaos* **10**, 427–469.

Kuznetsov, Y. A. [1998] *Elements of Applied Bifurcation Theory* (Springer Verlag), Second Edition.

Kwok, J. H. [1980] "Periodic orbits of the asteroidal type in the circular restricted three-body problem," in *AIAA/AAS Astrodynamics Specialist Conference*, AIAA-80-1654.

Lo, M. W., Williams, B., Bollman, W., Han, D., Hahn, Y., Bell, J., Hirst, E., Corwin, R., Hong, P., Howell, K., Barden, B., & Wilson, R. [2001] "Genesis mission design," *J. Astronautical Sciences* **49**(1), 169–184.

Lust, K. [2001] "Improved numerical Floquet multipliers," *Int. J. Bifurcation and Chaos* **11**(9), 2389–2410.

Marchal, C. [1990] *The Three Body Problem* (Elsevier).

Markellos, V. [1981] "Bifurcations of planar to three-dimensional periodic orbits in the general three-body problem," *Celestial Mechanics* **25**, 3–31.

Meer, J.-C. v. d. [1985] *The Hamiltonian Hopf Bifurcation* (Springer-Verlag).

Meyer, K. R. [1973] "Symmetries and integrals in mechanics," in *Dynamical Systems*, ed. Peixoto, M. (Academic Press) pp. 259–272.

Meyer, K. R. [1981a] "Periodic orbits near infinity in the restricted n-body problem," *Celestial Mechanics* **23**, 69–81.

Meyer, K. R. [1981b] "Periodic solutions of the n-body problem," *J. Differential Equations* **39**(1).

Meyer, K. R. [1999] *Periodic Solutions of the N-Body Problem* (Springer Verlag).

Meyer, K. R. & Hall, G. R. [1999] *Introduction to Hamiltonian Dynamical Systems and the N-body problem* (Springer Verlag).

Meyer, K. R. & Schmidt, D. S. [2000] "From the restricted to the full three-body problem," *Transactions of the AMS* **352**(5), 2283–2299.

Michalodimitrakis, M. [1978] "A new type of connection between the families of periodic orbits of the restricted problem," *Astronomy and Astrophysics* **64**, 83–86.

Montgomery, R. [1997] The 3-body problem. Lecture Notes, CIMAT, Guanajuato, Mexico.

Moore, C. [1993] "Braids in classical gravity," *Phys. Rev. Letters* **70**(24), 3675–3679.

Muñoz-Almaraz, F. J., Freire, E., Galán, J., Doedel, E. J., & Vanderbauwhede, A. [2002] "Continuation of periodic orbits in conservative and Hamiltonian systems," submitted.

Murray, C. D. & Dermott, S. F. [1999] *Solar System Dynamics* (Cambridge University Press).

Papadakis, K. E. & Zagouras, C. G. [1992] "Bifurcation points and intersection of families of periodic orbits in the three-dimensional restricted three-body problem," *Astrophysics and Space Science* **199**, 241–256.

Poincaré, H. [1899] *Les Méthodes Nouvelles de la Mécanique Céleste* (Gauthier-Villars).

Poincaré, H. [1993] *New Methods of Celestial Mechanics, Volumes 1-3*, American Institute of Physics. edited by D.L. Goroff.

Ragos, O., Papadakis, K. E., & Zagouras, C. G. [1997] "Stability regions and quasi-periodic motion in the vicinity of triangular equilibrium points," *Cel. Mech. Dyn. Astron.* **67**, 251–274.

Rheinboldt, W. C. [1986] *Numerical analysis of parametrized nonlinear equations*, University of Arkansas Lecture Notes in the Mathematical Sciences (Wiley-Interscience).

Richardson, D. L. [1980] "Halo orbit formulation for the ISEE-3 mission," *J. Guidance and Control* **3**, 543–548.

Robin, I. A. & Markellos, V. V. [1980] "Numerical determination of the three-dimensional periodic orbits generated from vertical self-resonant satellite orbits," *Celestial Mechanics* **21**, 395–434.

Rodriguez-Canabal, J. & Hechler, M. [1989] "Orbital aspects of the SOHO mission design," in *Orbital Mechanics and Mission Design*, AAS 89-171. pp. 347–356.

Roy, A. E. [1988] *Orbital Motion* (Adam Hilger).

Russell, R. D. & Christiansen, J. [1978] "Adaptive mesh selection strategies for solving boundary value problems," *SIAM J. Numer. Anal.* **15**, 59–80.

Schmidt, D. S. [1978] "Hopf's bifurcation theorem and the center theorem of Liapunov with resonance cases," *J. Math. Anal. Appl.* **63**, 354–370.

Sepulchre, J. A. & MacKay, R. S. [1997] "Localized oscillations in conservative or dissipative networks of weakly coupled autonomous oscillators," *Nonlinearity* **10**, 679–713.

Seydel, R. [1995] *From Equilibrium to Chaos. Practical Bifurcation and Stability Analysis*, Second Edition, (Springer Verlag, New York).

Simó, C. [1996] "Effective computations in Hamiltonian dynamics," in *Cent ans après les Méthodes Nouvelles H. Poincaré* (Société Mathématique de France) pp. 1–23.

Simó, C. [2000] "New families of solutions in n-body problems," in *Proceedings ECM 2000, Barcelona.*

Simó, C. [2001a] "Consecutive quasi-collisions in the planar circular RTBP," Technical report, Departament de Matemàtica i Anàlisi, Universitat de Barcelona.

Simó, C. [2001b] "Periodic orbits of the planar n-body problem with equal masses and all bodies on the same path," Technical report, Departament de Matemàtica i Anàlisi, Universitat de Barcelona.

Simó, C. [2002] "Dynamical properties of the figure eight solution of the three-body problem," *Contemporary Mathematics* **292**, 209–228.

Strizzi, J. D., Kutrieb, J. M., Damphousse, P. E., & Carrico, J. P. [2001] "Sun-Mars libration points and Mars mission simulations," in *AAS/AIAA Space Flight Mechanics Meeting*, AAS 01-159.

Stuchi, T. J., Antunes, A. C. B., & Andreu, M. A. [2000] "Muonic helium atom as a classical three-body problem," *Phys. Rev E* **62**, 7831–7841.

Szebehely, V. [1967] *Theory of Orbits: The Restricted Problem of Three Bodies* (Academic Press).

Vanderbauwhede, A. [1982] "Families of periodic orbits for autonomous systems," in *Dy-*

namical System II, eds. Bednarek, A. & Cesari, L. (Academic Press) pp. 427–446.

Viswanath, D. [2001] "The Lindstedt-Poincaré technique as an algorithm for computing periodic orbits," *SIAM Review* **43**, 478–495.

Zagouras, C. G. [1985] "Three-dimensional periodic orbits about the triangular equilibrium points of the restricted problem of three bodies," *Cel. Mech. Dyn. Astron.* **37**, 27–46.

Zagouras, C. G. & Kazantzis, P. G. [1979] "Three-dimensional periodic oscillations generating from plane periodic ones around the collinear Lagrangian points," *Astrophysics and Space Science* **61**, 389–409.

Zufiría, J. A. [1987] PhD thesis, Applied Mathematics, California Institute of Technology.